NIST-GCR-89-564

A Validated Furniture Fire Model with FAST (HEMFAST)

Mark A. Dietenberger

University of Dayton
Research Institute
Dayton, OH 45469

December 1988

Issued June 1989

Notice

————

This report was prepared for the Center for Fire
Research of the National Institute of Standards and
Technology under Grant Number 60NANBSD0556. The
statements and conclusions contained in this report
are those of the authors and do not necessarily
reflect the views of the National Institute of
Standards and Technology or the Center for Fire
Research.

NIST-GCR-89-564

A Validated Furniture Fire Model with FAST (HEMFAST)

Mark A. Dietenberger

University of Dayton
Research Institute
Dayton, OH 45469

National Bureau of Standards became the
National Institute of Standards and Technology
on August 23, 1988, when the Omnibus Trade and
Competitiveness Act was signed. NIST retains
all NBS functions. Its new programs will encourage
improved use of technology by U.S. industry.

Prepared for
U.S. DEPARTMENT OF COMMERCE
National Institute of Standards and Technology
National Engineering Laboratory
Center for Fire Research
Gaithersburg, MD 20899

U.S. DEPARTMENT OF COMMERCE
Robert Mosbacher, Secretary
NATIONAL INSTITUTE OF STANDARDS
AND TECHNOLOGY
Raymond G. Kammer, Acting Director

Notice

This report was prepared for the Center for Fire
Research of the National Institute of Standards and
Technology under Grant Number 60NANBSD0556. The
statements and conclusions contained in this report
are those of the authors and do not necessarily
reflect the views of the National Institute of
Standards and Technology or the Center for Fire
Research.

UDR-TR-88-136

A VALIDATED FURNITURE FIRE MODEL WITH FAST (HEMFAST)

MARK A. DIETENBERGER

UNIVERSITY OF DAYTON
RESEARCH INSTITUTE
DAYTON, OHIO 45469

DECEMBER 1988

FOREWORD

This final technical report describes the work accomplished during the period from 30 July 1987 through 30 September 1988 by the University of Dayton Research Institute (UDRI) under Grant No. 60NANBSD0557 for the National Institute of Standards and Technology. Dr. Vytenis Babrauskas of the Fire Measurement and Research Division, Center of Fire Research was the technical monitor.

The efforts reported here were performed by the principal investigator, Mark A. Dietenberger, a full-time member of the Structural Integrity Division of UDRI. Dr. A. M. Rajendran, head of the Analysis and Computation group provided project direction and Dr. Joseph P. Gallagher, head of the Structural Integrity Division served as the program manager. Ms. Joanda D'Antuono was responsible for typing and assembling the quarterly progress reports and this final technical report.

ABSTRACT

This technical document reports on the validation of the furniture fire model with the furniture calorimeter data and on the restructure of the program 'HEMFAST'. Significant restructuring of the model and its code resolve various problems associated with the first verison of HEMFAST. Comprehensive descriptions of the current model and its code structure benefit the HEMFAST users. The descriptions include: (1) data processing of the bench scale fire tests database, (2) effective time integrations of surface temperatures, flame spreads, and burn time, (3) effective coupled solutions of pyrolysis rates, burnrates, soot production, and thermal radiation, and (4) the effective interfacing between the furniture fire model and FAST. The model is validated with fire tests for a 4-cushion mockup fire with three different fabric/foam cushion types. The comparisons include: (1) burn area fractions of each cushion as a function of time, (2) burnrate of the mockup as a function of time with fire test data from the furniture calorimeter, (3) mass loss rate of the furniture as a function of time, and (4) the overall levels of soot production.

TABLE OF CONTENTS

LIST OF ILLUSTRATIONS

LIST OF ILLUSTRATIONS (concluded)

NOMENCLATURE

A_i	surface element area (m^2)
C	material heat capacity (J/g°K)
C_o	constant coefficient in Eq. (17)
C_{pa}	air heat capacity (J/g°K)
c	1st calibration constant for burn history
D	hydraulic diameter of the flame base (m)
d	2nd calibration constant for burn history
δ	material thickness (m)
δ_f	conductive thermal length (m)
F_{co}	carbon monoxide mass fraction of fuel
F_j	mass fraction of combustion product, j
$F_{s,exit}$	soot mass fraction of fuel from cone calorimeter
G	time stretching parameter
g	gravitational acceleration (m/s^2)
H_c	heat of reaction of carbon (kJ/kg)
H_{co}	heat of reaction of carbon monoxide (kJ/kg)
$\dot{h}_{cone}$	chemical heat release flux from cone calorimeter (kW/m^2)
$\dot{h}_{st}$	quasi-stoichometric heat release flux (kW/m^2)
$\dot{h}^*$	scaled heat release flux (-)
k	material thermal conductivity (kW/Km°)
k_a	air thermal conductivity (kW/m°K)
$k_{s,flame}$	soot absorption coefficient in flame (m^{-1})
$k_{s,max}$	maximum soot absorption coefficient for the material (m^{-1})
L	mean beam length of the flame (m)

$\dot{M}_{fuel}$ mass release rate into the flame (kg/s)

$\dot{m}_{fuel}$ material mass loss flux from cone calorimeter (kg/m^2s)

$\dot{m}^*$ scaled mass release flux (g/J)

Q heat release rate of fire (kW)

Q_c total heat release rate of flame (kW)

Q_{c_p} heat release rate from horizontal surfaces (kW)

Q_{c_w} heat release rate from inclined surfaces (kW)

q_c convective surface heat flux (kW/m^2)

q_f gaseous surface conductive heat flux at flame front (kW/m^2)

q_o scaled heat flux constant parameter (kW/m^2)

q_{rb} surface radiative heat flux emitted from material (kW/m^2)

q_{rf} surface radiative heat flux from flame in cone calorimeter (kW/m^2)

q_{ri} surface radiative heat flux from cone heater (kW/m^2)

q_s net surface heat flux (KW/m^2)

ρ material density (kg/m^3)

ρ_a air density (kg/m^3)

s surface distance from the flame front (m)

s_e preheated distance (m)

σ_p^e soot extinction area (m^2/kg)

σ_s^e specific soot extinction area (m^2/kg)

T^* scaled time (effective heat release per area) (kJ/m^2)

T_f temperature in combustion zone of diffusion flame (°K)

T_{ig} surface ignition temperature (°K)

T_s material surface temperature (°K)

T_o initial surface temperature (°K)

t time (seconds)

V_a opposed air speed at flame front (m/s)

V_f flame front quasi-steady speed (m/s)

Y_w wall pyrolysis zone width (m)

Z_f merged pool/wall fire height (m)

Z_{f_p} averaged visible pool fire height (m)

Z_{f_r} solid flame height (m)

Z_{fw} averaged visible wall fire height (m)

Z_w wall pyrolysis zone length (m)

SECTION 1

INTRODUCTION

1.1 BACKGROUND

The evolution of compartment fire models in recent years has included new models of the fire source, of which the model for Heat and Mass Transport of Furniture Fire, Smoke, and Toxic Gases (HEMFAST) is one example. The compartment fire models, such as FAST [1], utilize the distinct gas zones concept as a compromise between a network model and a finite difference model. That is, basic equations describe the mass, momentum and energy transfer from zone to zone in a fire driven environment. The numerical solution of these equations were shown to be both practical and adequately detailed. There was a need, however, to develop better models of a self-consistent fire on a general mockup and of thermal radiation heat exchanges between all surfaces and gas zones.

The motivation for the furniture fire model was two-fold. The first was to predict full scale fire tests using only bench scale fire data. The second was to make accurate predictions of the spread of fire, smoke and toxic gases for determining the hazard in various fire scenarios. Such an analytical tool has potential in reducing the number of costly full scale tests and in providing the fire protection community an improved predictive capability for fire hazard, particularly when evaluating new materials in a new environment.

The HEMFAST computer model provides dynamic, quasi-three-dimensional predictions of furniture fire growth and burnout in a room as well as of the spread of both nontoxic and toxic gases and smoke to other rooms. The HEMFAST model merges FAST with the Furniture Fire Model (FFM) as shown in Figure 1. The figure also shows the input and output of the combined models. The three-dimensional aspect of the HEMFAST model includes: mockups constructed of connected panels, several flame volumes attached to pyrolyzing polygonal bases and sides, a radiation heat exchange between facets of objects, flames, and gases, and the construction of multiple gas zones in a few rooms. The dynamic aspect of the model is a result of calculating the flame spreading in any direction on a mockup, the scaled burning history of mockup facets, the varying heat, fuel, and combustion products release rates, the temperature changes of mockup facets, walls, and gas layers, and the growth of the upper

INPUT →

FAST
● Room geometries
● Wall properties
● Room openings
● Fire Source ID

FFM
● Materials data from cone calori-meter and flame spread apparatus
● Ignition scenario

HEMFAST
FAST
(Gas Dynamics)
FFM
(Fire Spread and Thermal Radiation)

OUTPUT →

FAST
● Gas and wall temperatures
● Growth of upper gas layer
● Flashover of upper gas

FFM
● Regions of fire spread and damage
● Burnrate and combustion prod-ucts
● Surface and volume heat fluxes

Figure 1. The HEMFAST model

gas layer with combustion products. Almost any furniture material can
eventually be simulated in the model because of the model's reliance on the
effective scaling of the cone calorimeter data and of the flame spreading
data. All these features taken together make HEMFAST unique and promising.

1.2   OBJECTIVES AND ORGANIZATION

The main objectives of this report are to outline progress obtained
with: the validation of the furniture fire model with full scale fire tests,
the restructure of the program HEMFAST, and the comprehensive description of
the model for new potential users. Section 2 describes each physical process
considered in the Furniture Fire Model such as the material heating, flame
spreading, material pyrolysis, flaming combustion, flame shapes, and heat
tranfers. It is explained how each physical process is scaled from the bench
scale data to the full scale data as well as how they are utilized in the
HEMFAST calculation system. Section 3 describes the HEMFAST program
structure. The interfacing routines for merging FAST and FFM and the program
modules of FFM are explained. During the current contract period, significant
restructure of the computer code provided a relatively robust, well
structured, flexible and validated model. The validation of the HEMFAST model
with the furniture calorimeter fire tests of furniture mockups is described in
Section 4. Section 5 presents conclusions and recommendations.

This page intentionally left blank

SECTION 2
STRUCTURE OF HEMFAST MODEL

As previously described, HEMFAST merges FAST and FFM models. The
structure of FAST model is described fully in Reference 1. Thus, this report
concentrates on describing the structure of the Furniture Fire Model and its
interaction with the FAST model. The main objectives of the HEMFAST
development are to: (1) Improve the model predictions for the accelerative
growth of the fire from smoldering/ignition to a peak value and then the
gradual die-out as depending on a fire scenario. (2) Utilize only the cone
calorimeter database and the flame spreading data as the materials input data.
(3) Obtain an effective interface between FAST and FFM by achieving: minimal
changes to the FAST program, obtain reasonable computer time, maintain good
solution stability, and construct modular program units. The second HEMFAST
model version has mostly satisfied these objectives whereas the first version
of HEMFAST barely succeeded with the first objective and none on the other
objectives.

The construction of modular program units in FFM differed significantly
from other reported approaches because of our attempt to realistically
simulate an arbitrarily shaped fire on an arbitrarily shaped furniture. That
is, many researchers tend to treat a flame source as a modular program unit
with the idea of combining the various types of fire sources within a
compartment fire model. This approach has inherent inconsistencies as
follows.

In large fires, the thermal radiation field is highly coupled with
material pyrolysis rates underneath the flame. The thermal radiation is most
realistically analyzed in a single program module that considers the complete
environment of the multiple flames, the upper and lower gas layers, and the
radiating surfaces all with gray emissivities values. Additionally, the
thermal radiation field solutions must be coupled with the material pyrolysis
rate distributions controlling the flame size in order to avoid problems with
overall solution accuracy or stability. This feature is missing in some
compartment fire models. Another problem is how to consider the merging of
burning regions by flame spreading or thermal ignitions and the consequential
flame shape. Lastly, there must be some way of keeping track of the rising

virgin surface temperatures and of the burning material thicknesses as a function of time and location. It seemed logical and more general to organize program modules according to physical processes and construct general geometrics as a common denominator among the modules instead of organizing program modules according to separate fire sources and giving a complete sequence of physical processes for each such module.

Previously [3,4], we determined that to utilize the cone calorimeter data and the flame spread data, a model of a physical process must be analyzed in two phases. The first phase is the processing of the basic database to derive material parameters for flame spreading and to derive scaling variables corresponding to the cone calorimeter measured variables. The second phase uses the processed data from phase one as input to the predictive fomulae for the various physical processes. The program module for each physical process was carefully organized to obtain the optimal numerical solution as part of phase two. The structure of the HEMFAST model thus contains two analysis phases. The first derives the FFM input database and the second is the HEMFAST calculation system.

2.1 STRUCTURE OF FFM INPUT DATABASE

Figure 2 presents the organization of the FFM input database. The cone calorimeter data and the flame spread data as described in Reference 5 are organized under FFM basic data. From this basic database are derived the databases as inputs to the various formulae of the physical processes in the HEMFAST calculation system.

The first derived database consists of the material parameters for ignition and flame spread. The basic flame spread data typically consist of time to ignition and of the flame spread rate on a horizontal sample under varying irradiances. The formulae for thermal ignition and flame spread rate are fitted to this basic data to derive the corresponding material parameters. The curve fitting routines are still separate from the HEMFAST code because they are too complex and need to be replaced by a simpler curve fitting routine based on a more effective model of flame spreading.

The next two derived databases in Figure 2 are the scaling of quasi-stoichometric heat release rate and the scaling of fuel pyrolysis rate as a
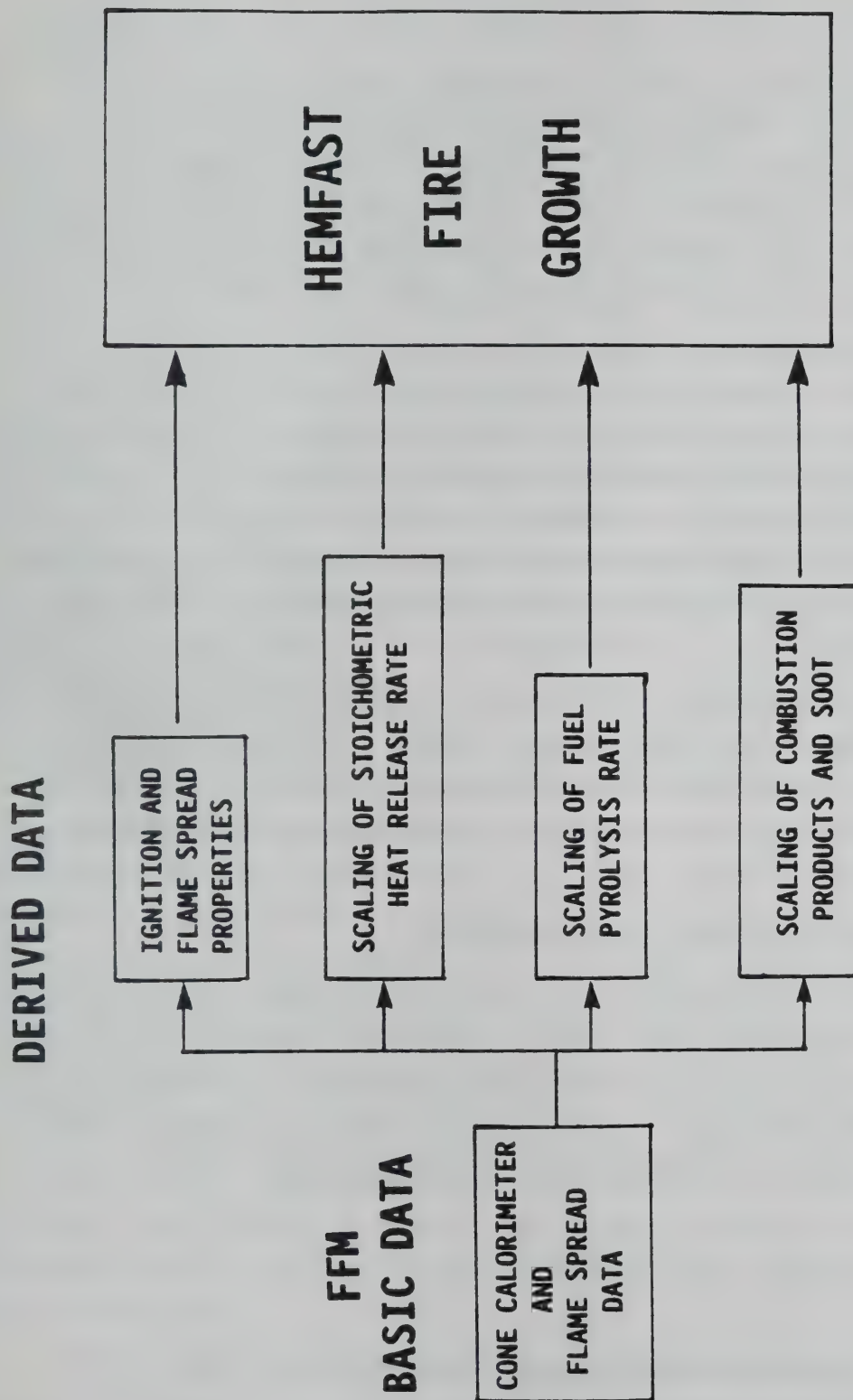
Figure 2. Structure of FFM input database

function of burn time for a given material. Three constants for scaling the basic heat and mass release rates, explained in paragraph 2.1.2, are presently determined in a user interactive graphics program separate from the HEMFAST code. These constants along with the data processing routines from the interactive graphics program are used by the HEMFAST code to create the database of scaled heat and mass release rates as a function of material burn history. The constants for scaling the basic data will eventually need to be obtained without resort to the user interactive graphics program.

The last derived database contains the scaling of combustion products and of soot mass fractions as a function of burn time; it is explained more fully in subsection 2.1.3. The derived two soot parameters, the maximum soot absorption coefficient and the specific soot extinction areas, are presently treated as constants, but should eventually be obtained as a function of material burn history. These parameters are used in the formulae to calculate the soot mass fraction and the soot extinction area in the fire plume as a function of burn time.

Despite the inadequancies in the current data processing routines, the current FFM derived database is sufficient to obtain a validation of the HEMFAST model with the furniture materials selected in Section 4. A more detailed explanation of the current modules for modeling physical processes during the first phase follows.

2.1.1 Ignition and Flame Spread Properties

In our earlier report [2], it was confirmed that the fabric/foam cushion and the PMMA materials have the following time to ignition and flame spread rate properties. The fabric/foam cushion behaves as a thermally thin material and the PMMA behaves as a thermally thick material. Thus the surface temperature of a thermally thin material is evaluated by the formula,

$$T_s = T_o + \int_o^t \frac{q_s(t-\tau)\ d\tau}{\rho c \delta} \tag{1}$$

while the surface temperature of a thermally thick material is evaluated by the formula,

$$T_s = T_o + \int_o^t \frac{q_s(t-\tau)\ d\tau}{\sqrt{\pi\ k\rho c\tau}} \tag{2}$$

The net surface heat flux, q_s, due to net radiative heating and to convective cooling is the heat load on the material. The surface temperature response of the thermally thin material is mediated by the characteristic thermal thickness, $\rho c\delta$, while that of the thick material is mediated by the thermal inertia, $k\rho c$. The numerical integration of these two equations can be done by a predictor-corrector scheme, but unacceptably small time steps may be required to maintain accurate solutions due to the surface heat flux also being a function of the surface temperature. Thus the predictor equation for Eq. (1) was revised to exponentially approach the equilibrium temperature for a constant irradiance level at any time increment chosen (see Reference 4). This will prevent a very thermally thin material from obtaining unreasonable surface temperature values. Equation (1) also has an analytical solution for an exponentially decaying irradiance flux as a function of elapsed time, $t-\tau$ (see Reference 2). The numerical integration of Eq. (2) was effectively addressed in the Harvard Computer Fire Code [6]. It is noted, however, that Eq. (2) has an analytical solution for a constant or an exponentially decaying irradiance flux (see Reference 2).

By setting the surface temperature, T_s, to the ignition temperature and the integrated time, t, to the ignition time, it is possible to curve fit the analytical solutions to the data of the time to ignition versus irradiance flux. The values for the ignition temperature and the effective thermal thickness of the thermally thin materials and values for the ignition temperature and the thermal inertia of the thermally thick materials were obtained in this way (see Reference 2). More generally, a material could be porous, finitely thick or layered, which may imply neither thermally thin or thick behavior. Approximate analytical solutions were obtained recently for these type of materials exposed to constant or exponentially decaying heat fluxes. They can eventually be included in the furniture fire model with minor modifications.

Many studies of flame spread often consider the deRis [7] classical solutions for the opposed flow flame spread over both thermally thin and thick materials due to the heating from the diffusion flame anchored at

the pyrolysis front. Recently the effect of finite chemical kinetics was included by empirically adjusting the flame spread rate as a function of the Damkohler number [8-10]. However, we only have access to the time to ignition and to the flame spread rate data in the air and that we may have to contend with non-ideal materials. At the other extreme, one approach to modeling flame spread is to define a surface element ignition "state" when the calculated surface temperature reaches ignition temperature. The heat transfer from the anchored diffusion flame to the heated virgin surface would still need to be calculated. This approach becomes impractical when we consider the small heating length (in millimeters) derived in the deRis flame spread model. That is, it is not practical to numerically construct surface elements smaller than millimeters in order to properly resolve the heating from the anchored diffusion flame. Thus, there must be new ways of applying the classical solutions of flame spread to our problem. Wichman [11] demonstrated a simplified flame spread model that gives similar results as deRis analysis. One result of Wichman's analysis is equivalent to a coordinate transformation,

$$s = V_f(t - \tau) \qquad , \tag{3}$$

where s is the surface distance from the flame front and V_f is the quasi-steady flame speed. This permits a consideration of a surface heat flux distribution from the flame front to the preheated distance, s_e, with the flame spread rate treated as constant over s_e. Substituting into Eq.(1) and solving for the flame spread rate of the thermally thin material, we obtain a good approximation (see Reference 2),

$$V_f = \frac{\sum\limits_{k} q_k s_k}{(\rho c \delta)(T_{ig} - T_e)} \qquad , \tag{4}$$

where the numerator components q_k and s_k are directly constructed from the surface heat flux distribution as shown in Figure 3. Likewise for the thermally thick material we obtain a good approximation,
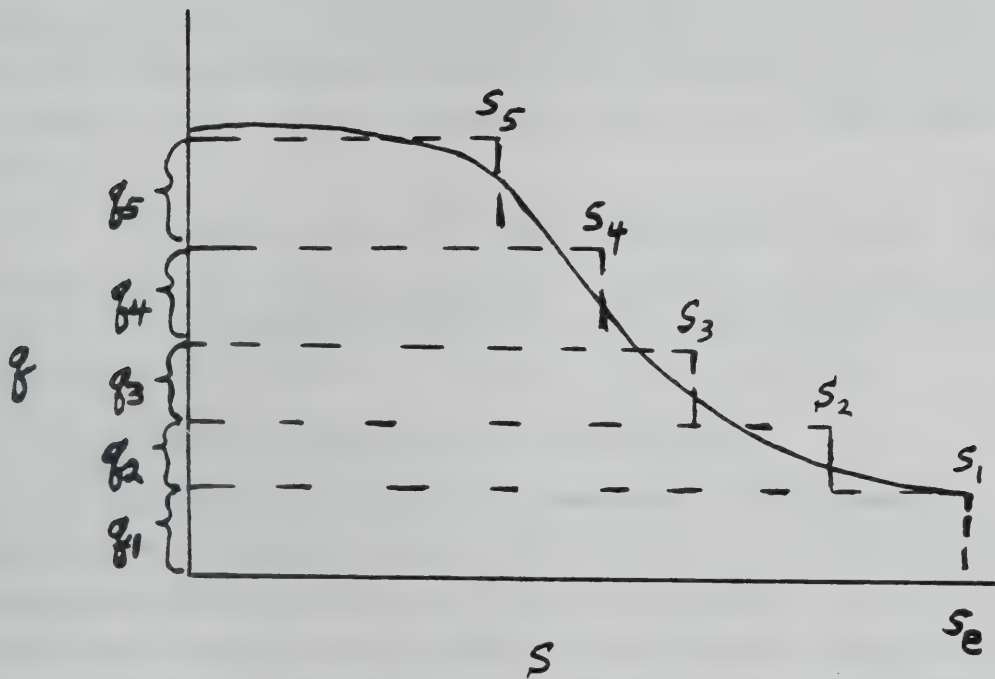
Figure 3.   Construction of q_k and s_k from heat flux
distribution, $q = f(s)$, fixed ahead of the
flame front at speed V_f

$$V_f = \left(\frac{\sum_k q_k \sqrt{4s_k/\pi}}{\sqrt{k\rho c}\,(T_{ig} - T_e)} \right)^2 \qquad (5)$$

These two equations have many possibilities. As one example, a correspondence with deRis results can be obtained by assuming a surface conductive heat flux as a decreasing exponential function of s. Then we convert the summation to an integral and set the ignition temperature to the vaporization temperature. The result for the gaseous surface conductive heat flux at the flame front is,

$$q_f = (\rho_a C_{pa} V_a)\,(T_f - T_{ig})/\sqrt{2} \qquad (6)$$

and the exponential decay length (i.e., the thermal length) is,

$$\delta_f = 2\,k_a/(\rho_a C_{pa} V_a) \qquad (7)$$

A generalization to deRis theory would require assuming that the diffusion flame is anchored to the critical ignition location in the fuel/air mixture rather than at the pyrolysis front. Thus the ignition temperature and the materials properties derived from the time to ignition data can be used also in the flame spread rate equations. One useful result for thermally thin materials is that the numerator in Eq. (4) is a constant regardless of the opposed air velocity unless the flame or the ignition temperatures are affected by the air environment.

The other source for surface heat flux distribution ahead of the flame front is the thermal radiation from the plume of the anchored diffusion flame and from other burning regions. Equations (4) and (5) can consider explicitly the two separate thermal radiation sources. The thermal radiative heat fluxes from other burning regions can be treated as a constant during the preheated length, s_e. The radiative flux from the adjacent fire plume can be modeled as a decreasing exponential function of s. The thermal radiation analysis of the HEMFAST model was designed to accommodate the above radiative heat flux distribution for flame spreading.

Thus any flame spread data must be examined carefully for two factors. The first is to determine if the material can be treated as thermally thin or thick, or even neither. This is done by curve fitting the different formulaes to the time to ignition versus irradiance data and selecting the one giving the best fit. The other factor is to sort the conductive heating separately from the radiative heating in the numerator terms of the flame spread formulae. One way to do the sorting is to use the HEMFAST code itself to calibrate the conductive heating contribution to the opposed flow flame spreading on a horizontal furniture cushion. This in fact was the approach necessary in the model validation with the furniture calorimeter.

The surface heat flux distribution for the upward flame spread was obtained from the data collected and correlated by Quintiere, Harkleroad, and Hasemi [12]. Equation (4) is then used for flame spreading on the fabric/foam cushions and Eq. (5) is used for the thick PMMA.

2.1.2   Scaling of Heat and Mass Release Rates

The need for scaling the heat and mass release rates versus scaled time can be ascertained from Figures 4a and 5a, which are plots of the corresponding cone calorimeter data of a typical fabric/foam cushion at three irradiance levels. The furniture fire in general will start at low irradiance levels at ignition and then reach high irradiance levels at the peak burnrate at a later time. There is a real problem in interpolating or extrapolating the data in Figures 4a and 5a to the conditions representative of the furniture fire. A detailed model of the fuel pyrolysis and the heat release rate to address this problem is avoided for two practical reasons. The data shown seem to imply that some complex processes are not readily simulated even by the most advanced detailed model. Secondly, the detailed models take up too much computer time, particularly when several surface elements are used in the model geometry. The alternative approach is to formulate a scheme to rescale the data for use in the furniture fire model.

Last year's report [3] described successful scaling techniques for the heat and mass release rates, which are summarized below. The key concepts for scaling were to develop variables similar to quasi-stoichometric heat of combustion and an effective heat of pyrolysis as a function of
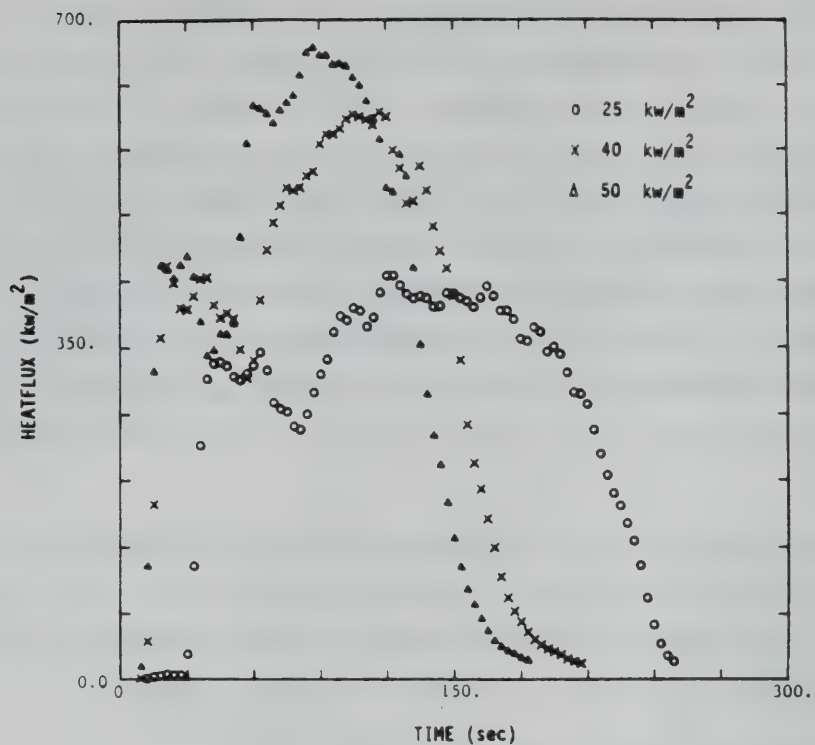
Figure 4a.   Original data of heat release flux versus
time for LO fabric/FR PU foam material
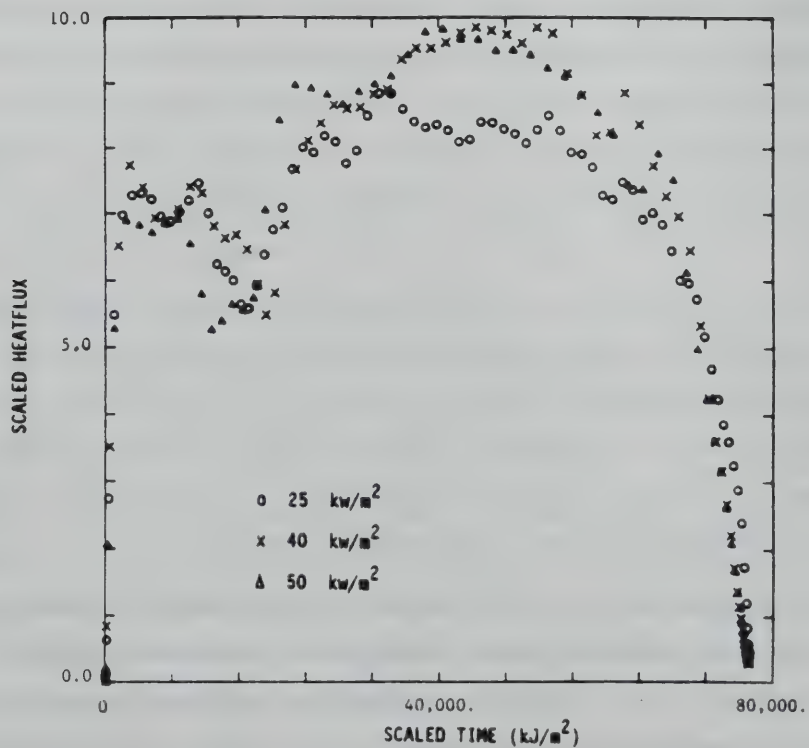
Figure 4b.   Correspond scaled heat release flux versus
scaled time for LO fabric/FR PU foam material
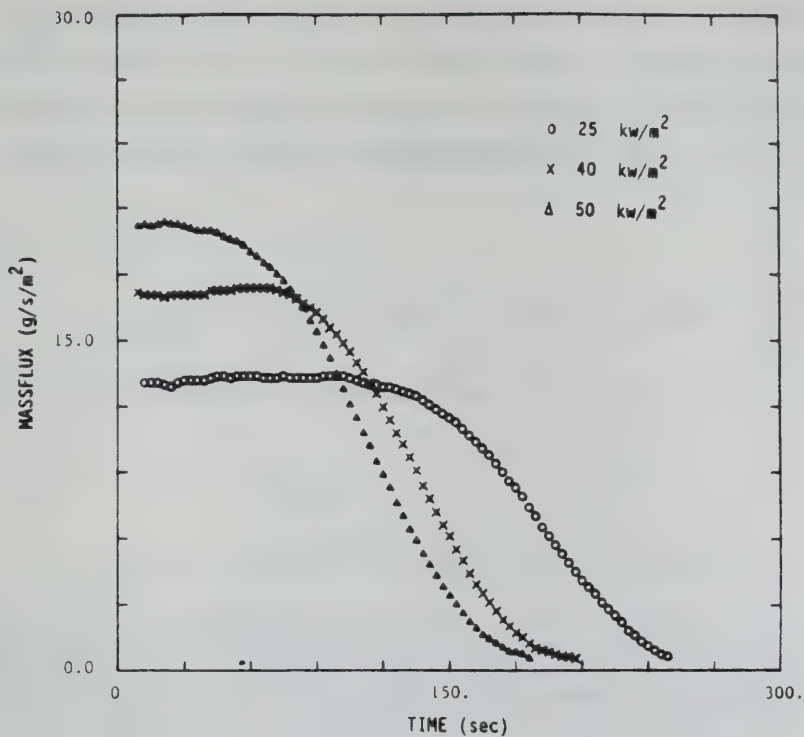
Figure 5a.   Original data of heat release flux versus
             time for LO fabric/FR PU foam material
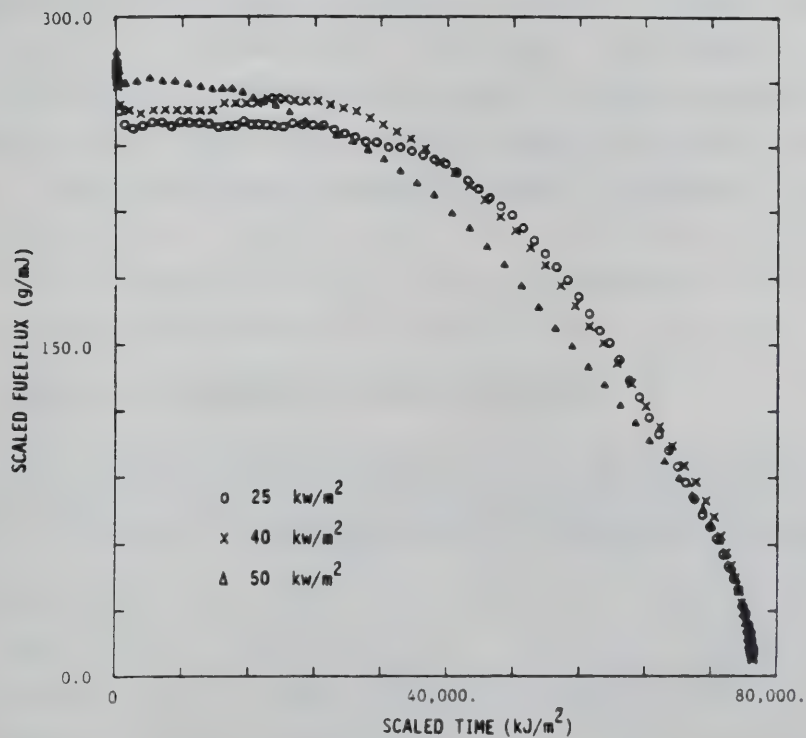
Figure 5b.   Correspond scaled heat release flux versus
             scaled time for LO fabric/FR PU foam material

material burn history. The processing of the cone calorimeter data is as follows. The measurements of the chemical heat release flux, the fuel mass loss flux, the soot mass fraction, and the mass fraction of carbon monoxide as a function of time are used to obtain the quasi-stoichometric heat release flux as in,

$$\dot{h}_{st} = \dot{h}_{cone} + \dot{m}_{fuel} \ (F_{s,exit} \ H_C + F_{CO} \ H_{CO}) \ .\qquad(8)$$

The net surface heat surface flux on the material sample is given by,

$$q_s = q_c + q_{rf} + q_{ri} - q_{rb} + q_o \quad , \qquad (9)$$

where the convective heat flux and the radiative heat fluxes from the flame, the attenuated cone heater, and the burning surfaces are considered. The scaled heat flux constant parameter, q_o, accounts for systematic errors in the other heat flux terms and for other unaccounted physical processes. Such physical processes may include glowing combustion, radiation blocking by stagnant pyrolytic gases, or altered pyrolysis processes at elevated temperatures or irradiances. The scaled heat release flux is equivalent to the quasi-stoichometric heat of combustion divided by the effective heat of pyrolysis. The scaled mass release flux is equivalent to the inverse of the effective heat of pyrolysis. These are given by the equations,

$$\dot{h}^* = \dot{h}_{st}/q_s \qquad (10)$$

$$\dot{m}^* = \dot{m}_f/q_s \qquad (11)$$

The scaled time (or the burn history) was found to be best represented by an effective heat release per area as given by the following equations.

$$T^* = \int_o^t \dot{h}_{st} \ (1 + G) \ dt \qquad (12)$$

$$G = 0 \quad \text{for} \quad \int_o^t \dot{h}_{st} \, dt \le c \, Q_{ref} \, d/(1 + d)$$

$$\text{or} \quad \ge Q_e - c \, Q_{ref}/(1 + d) \tag{13}$$

$$G = (Q_{ref} - Q_e) / (Q_e - c \, Q_{ref})$$

$$Q_e = \int_o^{t_{end}} \dot{h}_{st} \, dt \tag{14}$$

$$Q_{ref} = T^* \quad \text{at} \quad t = t_{end} \tag{15}$$

G is a time stretching parameter that ensures the scaled burnout time is identical for the similar materials. These materials can have variations due to non-ideal material construction or to variability in foam thicknesses. Most likely these similar materials will have nearly the same burning behavior at the beginning and the ending part of their burn history. Thus the middle part of a material's burning history will be only affected by the time stretching parameter as controlled by the scaling parameters c and d. Reference 3 give a more detailed explanations of these parameters.

The results of using the scaling Eqs. (8) to (15) are shown in Figures 4b and 5b, which demonstrate the approximate collapse of the data into a single curve after optimizing the three scaling constants. Thus the data presented in Figures 4b and 5b permit arbitrary variations in the net surface heat flux and in the burning history in order to calculate the heat and mass release flux of the surface elements in the furniture fire model.

2.1.3   Scaling of Combustion Products and Soot

The cone calorimeter measures currently the amount of fire products such as CO_2, CO, H_2O, HC, HCl, and soot with sampling techniques as a function of time. The soot extinction area as a function of time is determined from the soot absorption coefficient, the volumetric flow rate, and the fuel mass loss rate as a function of time. The soot absorption coefficient is measured with a laser attenuation technique and the volumetric flow rate is obtained with the temperature and air velocity sensors. Our present database is from an earlier version of the cone calorimeter, which

only derived accurate values for the heat and mass release fluxes, the oxygen consumption rates, the product ratio of CO to CO_2, and the soot extinction areas as a function of time. In many cases the soot extinction area data was available to us only in certain forms, such as the averaged value or the peak value. The other combustion products was estimated by us assuming stoichometric conditions within the fire, as the water vapor for example. Thus the only two additional data plots of significance are the CO/CO_2 ratios and the soot extinction areas versus time as shown in Figures 6a and 7a, respectively.

The combustion products, excluding the soot, in the current model is scaled the same way as the mass release flux, i.e., through equations similar to Eq. (11). It is therefore assumed that Eqs. (10) and (11) and those for the combustion products are only a function of the burn history and of the oxygen concentration in the air. The scaling for soot production is different in the sense that it is also affected by the size of the flame and by the chemical heat of combustion for the fire. This is given by the following equations from Reference 4.

$$F_s = \sigma_p^e / \sigma_s^e \tag{16}$$

$$\sigma_{p,exit}^e = C_o \, k_{s,flame} \, (Q / \dot{M}_{fuel}) \quad \text{and} \tag{17}$$

$$k_{s,flame} \, L = \begin{cases} (1.5 \, k_{s,max} \, L)^{3/2} & \text{for } k_{s,flame} \, L < 0.3 \\ \\ (k_{s,max} \, L) & \text{for } k_{s,flame} \, L \geq 0.3 \end{cases} \tag{18}$$

It is assumed that the specific soot extinction area, σ_s^e, and the maximum soot absorption coefficient, $k_{s,max}$, are only functions of the material burn history and of the oxygen concentration in the air. These two soot parameters are temporarily treated as constants for our present cone calorimeter data. Equation (18) is equivalent to Bard and Pagni's [5] expression for the flaming soot absorption coefficient and was justified in Reference 4. The exiting soot extinction area is calculated with Eq. (17), which was derived in Reference 4. Equation (16) provides the soot mass fraction by definition and is plotted in Figure 7a. The soot mass flux, which
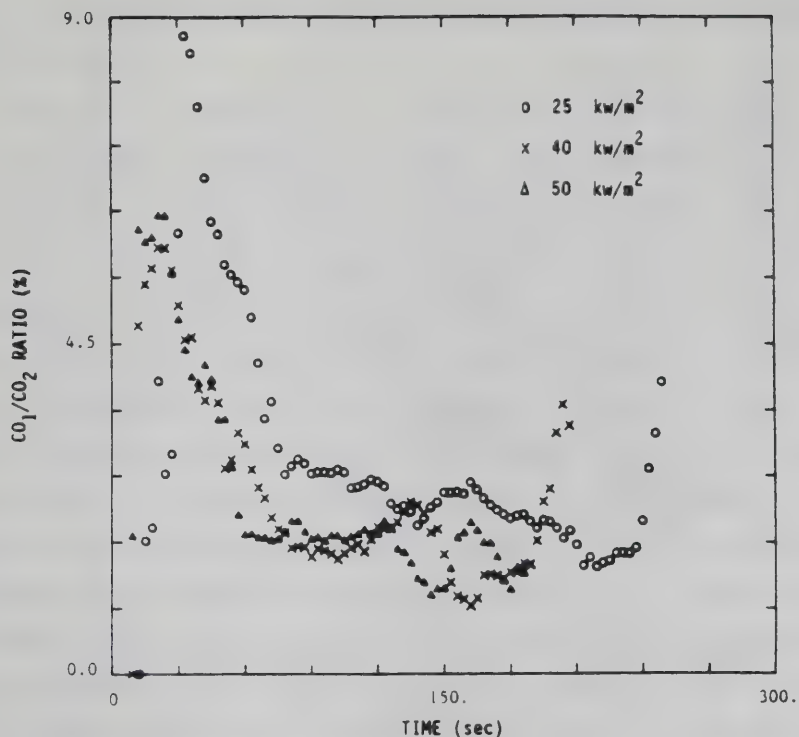
Figure 6a.   Processed data of CO to CO_2 mass ratio versus
scaled time for LO fabric/FR PU foam material
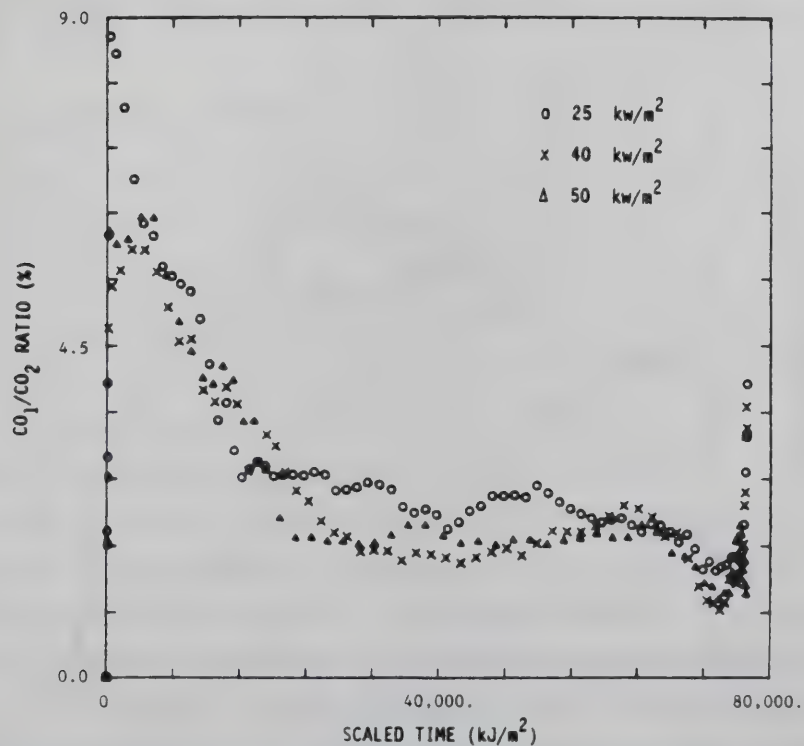
Figure 6b.   Processed data of CO to CO_2 mass ratio versus
scaled time for LO fabric/FR PU foam material
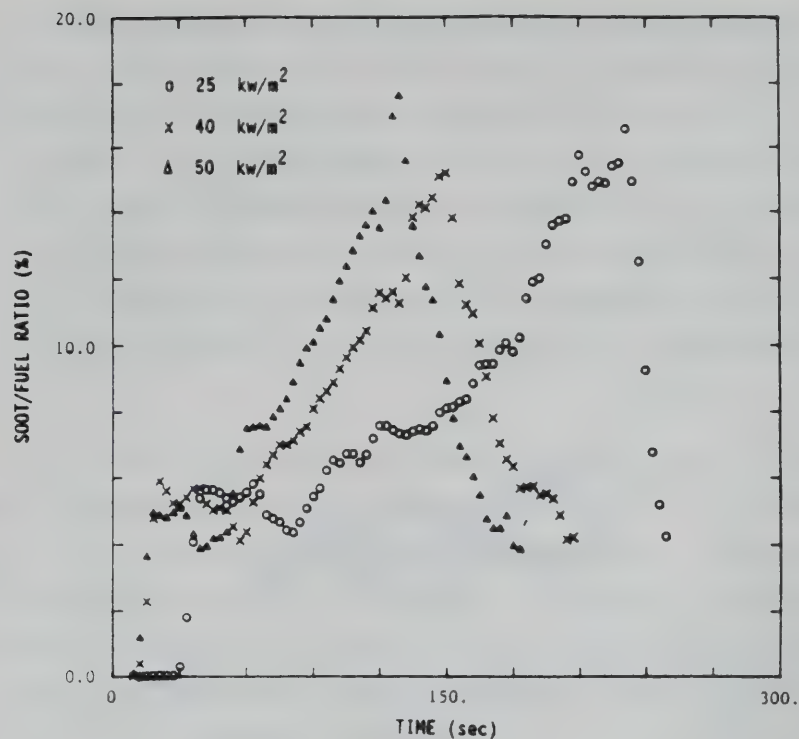
Figure 7a.   Calculated soot to fuel mass ratio versus
time for LO fabric/FR PU foam material
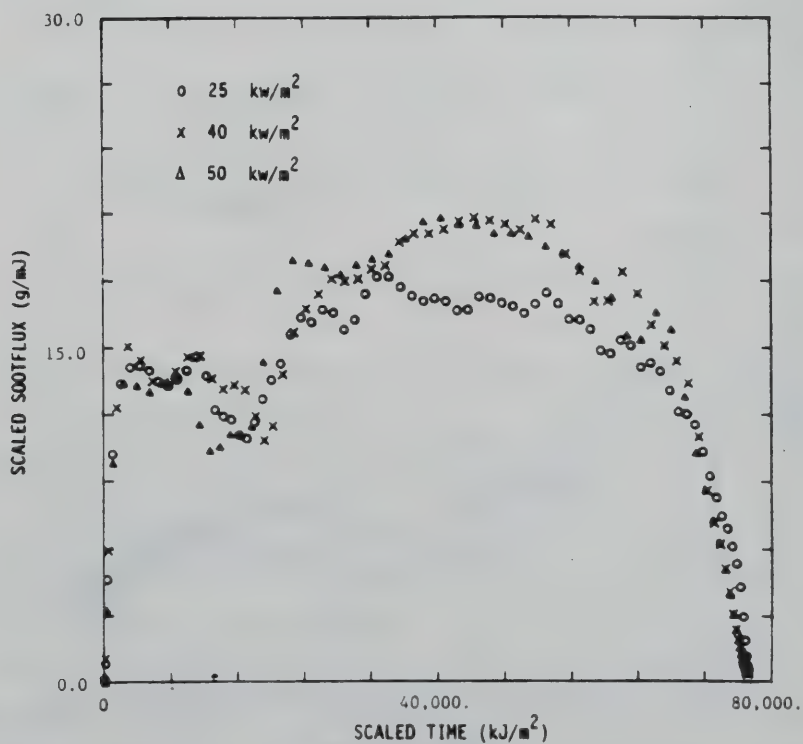
Figure 7b.   Calculated scaled soot mass flux versus
scaled time for LO fabric/FR PU foam material

2-16

is the product of Eq. (16) and (11), is plotted versus the material scaled burn time in Figure 7b.

Since the production of soot within the fire also affects the resulting chemical heat release rate of the fire which in turn determines the flame size, there is a certain degree of coupling between the variables of physical processes that must be accounted for in the model. The calculation of soot quantities in different forms is very significant and provides more important information than that from the other combustion products. In large fires, the soot dominates the thermal radiation, which in turn dominates the fuel pyrolysis and the consequential burning rate. The smoke leaving the fire is the major factor in hazard analysis. That is, the hot smoke can lead to human incapitation, obscuration, surface damage, and room flashover. The presence of smoke is a common means of fire detection. Thus any model that models the combustion processes in the fire source of a compartment fire model should include accurate calculations of soot production as having the most impact on fire hazard analysis. The scaling of soot production is therefore viewed to be as important (1) as determining the ignition and flame spread properties and as (2) scaling the heat and mass release fluxes. The scaling of other combustion products was kept simple in comparison to the scaling of soot production because of their lessen effect on hazard analysis.

2.2   HEMFAST CALCULATION SYSTEM

As noted above, there is a three fold coupling between the physical processes of fuel pyrolysis, soot production in the fire, and the thermal radiation due to the presence of the fire. It is also clear that additional, but different, couplings are involved in the thermal heating of virgin surfaces, the spreading of the fire base, and the burning history of a surface element. The thermal radiation field is the common denominator involved in these two sets of couplings between all physical processes. As a consequence, special attention was given to developing a thermal radiation analysis that could accommodate all the modeled physical processes and also be tolerant of the couplings between the variables. A modified form of the Hottel's thermal radiation model reported in Reference 2 was successfully implemented for a general mockup and fire, but the coupling variables had assumed fixed values. As these coupling variables began to be calculated as a function of time in

the furniture fire model, the solution accuracy, stability, and efficiency became a serious problem. This problem persisted even in the first version of HEMFAST.

The problem resolution resulted from analyzing the nature of couplings between variables describing the physical processes as shown in Figure 8. That is, the virgin surface temperature response, the flame spread, and the burn history changed slowly enough with time and are weakly coupled to each other such that they are integrated explicitly with time (top part of Figure 8). The predictor equations for these variables were reformulated to be more tolerant of the time step size. The other set of coupling variables, i.e., the fuel pyrolysis rates, the soot production, and the flame size along with the thermal radiation are strongly interacting and involve short time processes. These variables are solved in a convergent iterative scheme as shown in the lower part of Figure 8. Finally, the FAST output variables tended to have a relatively small influence on the furniture fire, so that in a particular time step, the furniture fire growth algorithms are executed first so as to have an immediate impact on FAST's predictions for the room. The results of implementing these changes in the structure of the HEMFAST model to significantly improve the model predictability was a complete overhaul of the program structure, which is described subsequently.

2.2.1   Prediction of Surface Temperature, Ignition, and Flame Spread

The implementation of the models of thermal ignition and flame spread in the furniture fire model is based on the geometrics chosen for the model. The three-dimensional vector algebra is fully utilized and is even required by the thermal radiation model to describe the geometries for the mockup, flame spreading regions, flame shapes, room shapes, and the gas zones.

A general but practical geometrical construction for the mockup is to simulate major mockup surfaces by trapezoidal panels which contain square-like surface elements. An example of a square panel with nine square elements to represent a mockup cushion is shown in Figure 9. The mockup shape is simulated by assembling the panels in the following way. First, a panel is defined in a neutral planar coordinate system. The corner points of the panel are defined in a counter clockwise direction around the normal vector of the
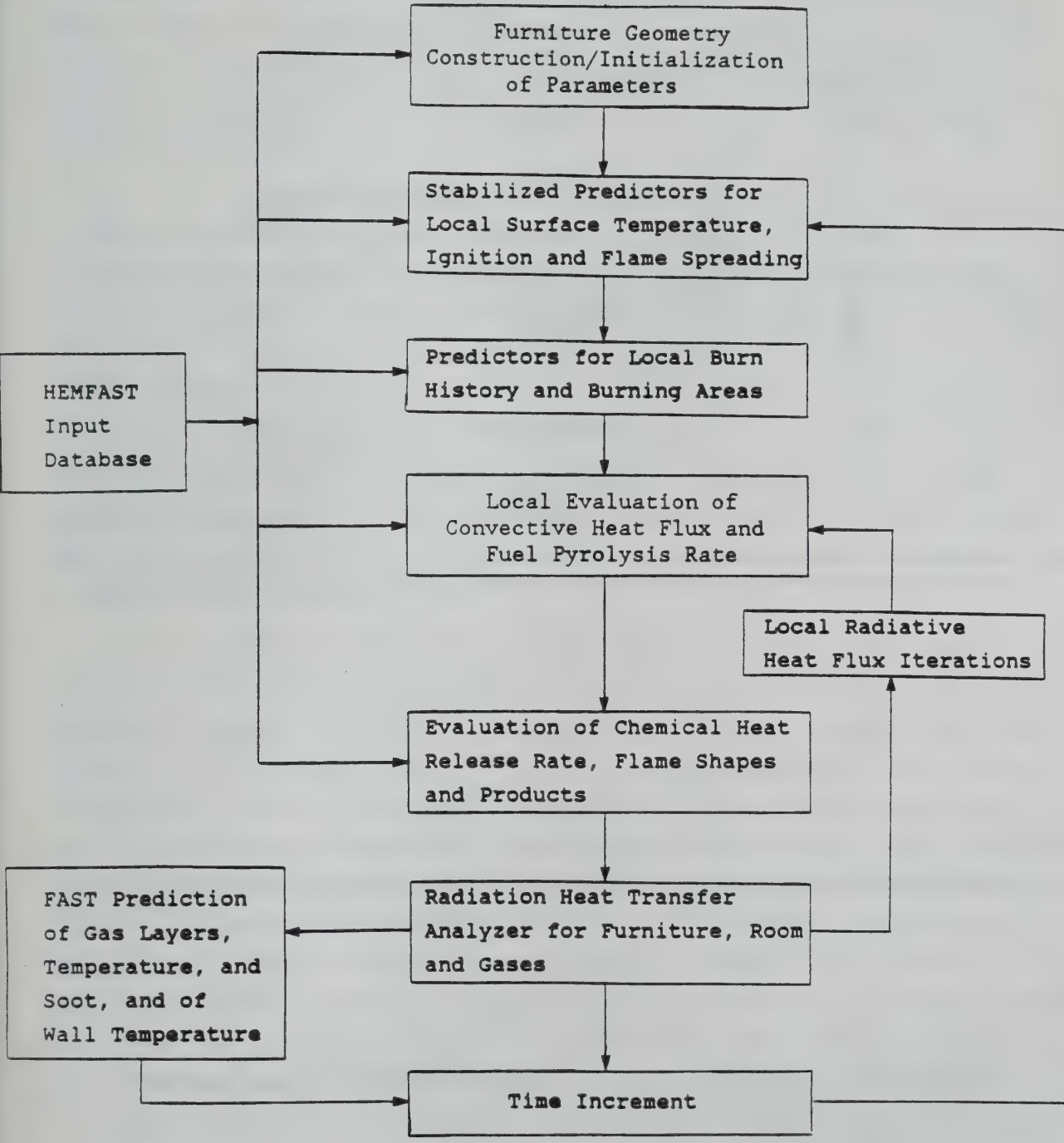
Figure 8. HEMFAST calculation system
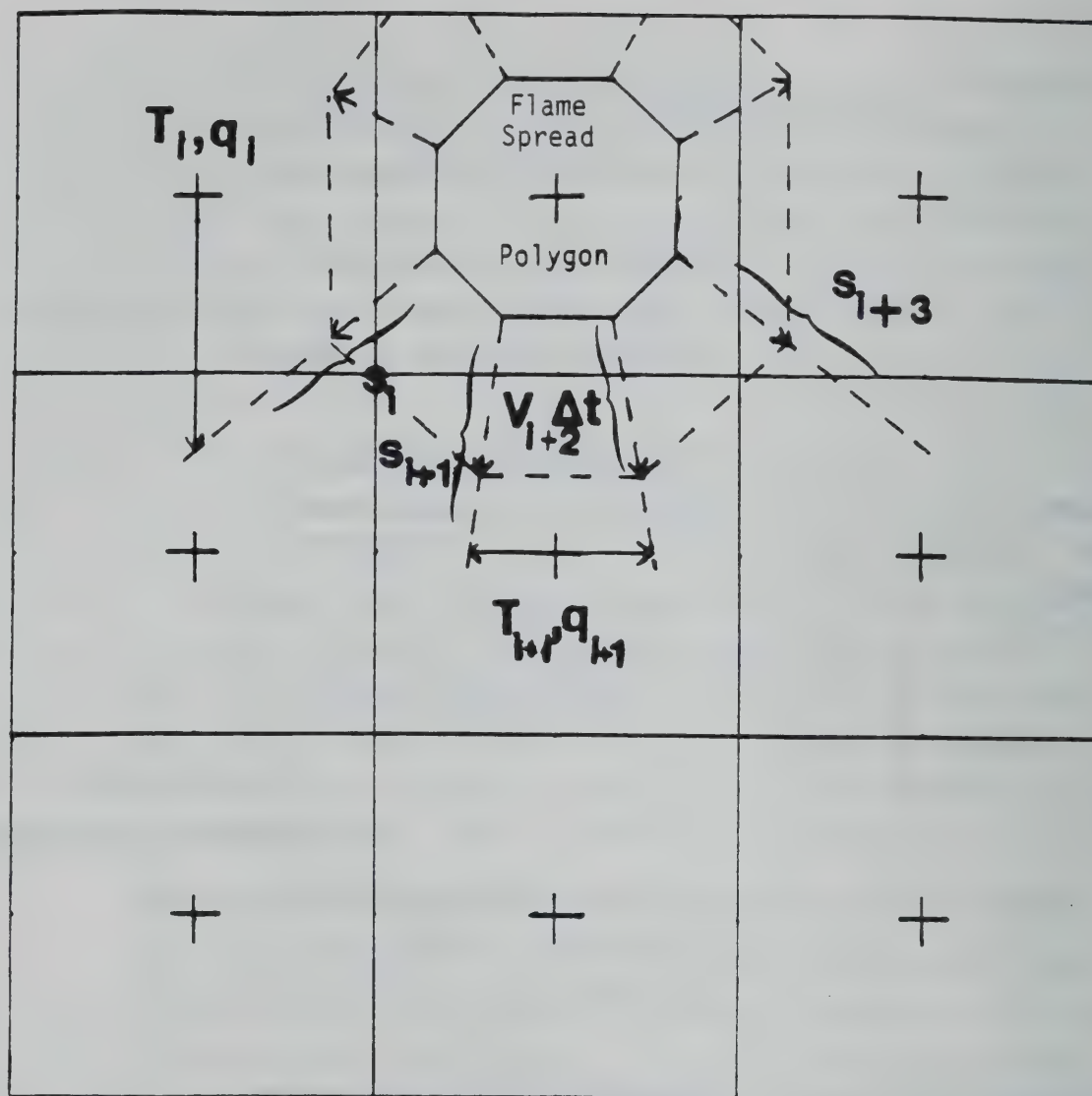
Figure 9.   HEMFAST flame spread procedure on a heated
            cushion panel

panel using inputs of panel's length and angle specifications. The additional input value of element area results in specifying the surface elements midpoint vectors, normal vectors, and actual areas. The input information for three-dimensional translation and rotation result in putting the panel in any place and in any orientation in the room. A mockup or even a number of mockups are constructed by repeated applications of the previous steps for the panel constructions.

The surface temperature and thermal ignition are thus predicted at each virgin surface element midpoint by the appropriate numerical integration of either Eqs. (1) or (2). The varying net surface heat flux is now obtained from the furniture fire model rather than prescribed by the cone calorimeter. The net radiative heat flux to the element midpoint is obtained from the thermal radiation model and the convective heat flux is obtained from the empirical relationships for natural convection. To ensure the surface temperature approaches its limiting equilibrium temperature, the surface temperature dependence within the surface radiative and the convective heat flux was separated out and was included in a quasi-analytical integration over a time step for Eqs. (1) or (2).

When the predicted surface temperature at a surface element over a time step exceeds critical temperatures, the model will redefine certain parameters in order to initiate the material burn history or a burning region or both at the surface element. If the critical temperature is the ignition temperature, then the following is implemented. The surface temperature is reset to the burning temperature, the remaining burning time in the time step is calculated, the surface element is labeled as burning, and the flame spread region is defined with the surface element. If the critical temperature is the pyrolysis temperature less than the ignition temperature, then the remaining "burning time" in the time step is calculated and a pyrolysis state is defined for the surface element. The definition of a pyrolysis state allows for the possibility of a material to decompose into gases not involved in flaming combustion at the surface element. If a surface element is already labeled burning or pyrolyzing and also the net surface heat flux, q_s, becomes negative, then the burn history is frozen and a surface temperature decrement over the time step is calculated instead. Conceptually, a fire suppression

and eventual re-ignition of a surface element can be analyzed through the effects on the net surface heat flux.

The opposed flow flame spread region is by definition the time integration of the flame spread rate in the direction normal to the flame front and along the surface. The assisted flow flame spread region on the other hand spreads along the fire plume direction. An octogon with its vertices moving outward as shown in Figure 9 seems to be a practical representation of the flame spread region originating at a piloted ignition point. An elongated eight sided polygon would be practical for a line ignition source. Each vertex of a polygon is represented by a three-dimensional vector sequenced in a counter-clockwise direction around the polygon normal vector. Thus the direction of the flame spread vector is a normalized cross product of the polygon normal vector with the vector between staggered vertices. The magnitude of the flame spread vector is then the flame spread rate multiply by the time step, unless it is cut short by intersection with the panel edge.

For the prediction of the flame spread rate, the preheated temperature and the heat flux distribution shown in Figure 3 are the additional parameters needed in Eqs. (4) and (5). The preheated temperature is taken to be the predicted surface temperature at the virgin surface element midpoint which is the closest to the vertex of a flame spread vector. The surface element midpoint is then extrapolated (parallel to the flame front) to the flame spread vector line to define the preheated length, s_e. The external radiative heat flux determined at the surface element midpoint is also extrapolated as a constant heat flux as part of the heat flux distribution in Figure 3. The radiant and the convective heat fluxes between the heated surface and the ambient air are included in the heat flux distribution by treating them as a product of a linearized heat transfer coefficient and the temperature difference between the air and the surface. The increase of external radiative heat flux from the distance s_e to the vertex point at $s=0$ due to the adjacent fire plume is modeled as a decreasing exponential function of s. Lastly, the conductive heat flux distribution from the anchored diffusion flame was described in the derivation of Eqs. (6) and (7). All these heat flux distributions are substituted into Eqs. (4) or (5) and the summations are converted to integrals. The Duhamel theorem and the Laplace

tranform are applied to obtain an explicit analytical expression for the flame spread rate.

The conductive heat flux distribution was not split into two parts as was done for the external radiant heat flux distribution for the following reasons. Its effective length, given by Eq. (7), is typically much smaller than a surface element size, which is the same magnitude as s_e on the average. Thus the conductive heat flux from the anchored diffusion flame barely affects the preheat temperature at the virgin surface element midpoint. Secondly, the source of this conductive heat flux is only from the direction of the adjacent flame front and tends to be well defined. Also, a minimum practical value of the flame spread rate is needed to initiate flame spreading from a point ignition source. The external radiative heat flux on the other hand tends to be long range as well as affected by other fire sources. Furthermore, the radiative heat flux tends to be miniscule at the beginning of the fire spread. The inclusion of the external radiative heat flux in preheating as well as in flame spreading should reduce the sensitivity of the flame spread rate to the surface element size and provide a approximate separation of the sources of external radiative fluxes.

The last features of the flame spreading procedure included in the model are the capability to merge overlapping burning regions and to create new burning regions in the adjoining panels as a result of flame spreading, thermal ignitions, or even new piloted ignitions. The three-dimensional vector algebraic analysis was again applied to implement these features. This analysis ensured the flame spread polygons are placed properly with their corresponding panels. Once all such polygons are in place and all previous surface elements parameters are updated and redefined, the burn histories of burning elements are calculated next.

2.2.2   Prediction of Local Burn History

As described in paragraph 2.1.2 and demonstrated in Figures (4) and (5), the burn history of a furniture material was sufficiently complicated that a practical prediction of material burning required rescaling the cone calorimeter data. Although Eqs. (8) to (15) have proven adequate for modifying the burn rate and the burn time for collapsing the data unto a single curve, it was not obvious how Eq. (12) for the burn history can be used

in the furniture fire model. The problem is made more clear by taking the scaled heat release flux as a function of the scaled burn history from Eq. (10) and substituting into Eq. (12) to get,

$$T^* = {_0}\!\int^t q_s(t) \; \dot{h}^*(T^*) \; (1 + G(T^*) \;) \; dt \qquad . \qquad (19)$$

Several difficulties can be found in the use of this equation. For one thing the scaled burn time is an integral-non-linear function of itself as well as being a function of real time. The integral itself in Eq. (12) is evaluated with a trapezoidal numerical integration to produce the scaled data in Figures 4b and 5b. The value of the net surface heat flux, q_s, is only available at the beginning of the time step for the HEMFAST calculation system shown in Figure 8. A practical alternative to Eq. (19) is its rearrangement to,

$$_{t_i}\!\int^{t_{i+1}} q_s(t) \; dt = {_{T_i^*}}\!\int^{T_{i+1}^*} dT^* / \{ \; \dot{h}^*(T^*) \; [1 + G(T^*) \;] \; \} \qquad . \qquad (20)$$

The right term of this equation utilizes the scaled data presented in Figure 4b and the left term uses the net surface heat flux derived in the furniture fire model as a function of time. The selection between the three data sets in the figure (i.e., circles, triangles and x's) is determined by the magnitude of the net surface heat flux. Thus Eq. (20) provides a one to one relationship between the real burn time, t_i, and the scaled burn time, T_i^*. The implementation of Eq. (20) in the HEMFAST calculation system involve a trapezoidal numerical integration of the right side of Eq. (20) and an euler numerical integration of the left side. Thus it was possible to keep the local burn history in step with the local real burn time in a simple way.

The receding depth of the burning material is assumed approximately proportional to the scaled burn time. The proportionality constant is the virgin material thickness divided by the ending scaled burn time (or the total quasi-stoichometric heat release per area of the material). If all the surface elements in a panel are burning, then the flame spread polygon is shifted to keep in planar contact with a nearest burning surface

element. When the flame spread polygon is finally shifted by an amount equal to the virgin material thickness the panel is removed from the mockup geometry.

The predictions of the surface temperatures, the flame spread polygons, and the burn histories are in essence the integrations of first-order ordinary differential equations which are assumed weakly coupled and non-stiff. Explicit integrations of these equations have so far presented no problems. If the coupling or stiffness of these equations become important, the HEMFAST calculation system can be modified to implement a stable first-order Diagonally Implicit Runge Kutta (DIRK) scheme [13]. The formulae that describe the combustion rate, the flame shapes, the soot production, and the thermal radiation on the other hand are a system of coupled nonlinear functions. Their solution is described below.

2.2.3   Local Convective Heat Flux and Fuel Pyrolysis Rate

An effective solution scheme developed has all the relevant variables except for the radiative heat fluxes involved in the fixed point iteration method. The values of the relevant variables are input in an effective Gauss-Seidel matrix solution of the Hottel's thermal radiation equations. The radiative heat fluxes thus obtained are used to modify the values of the relevant variables which are fed back into the thermal radiation equations. This process is repeated until convergence is obtained. The first step in the iteration, as shown in the middle of Figure 8, is the local evaluation of the convective heat flux and the fuel mass loss rate. The coupling between the fuel mass loss rate and the convective heat flux as well as the decoupling between the fuel mass loss rate and the burn history is better understood by rearranging Eq. (11) as,

$$\dot{m} = (q_c + q_r + q_o) \ \dot{m}^*(T^*) \quad . \tag{21}$$

Since the scaled burn time has been obtained from the solution of Eq. (20) and the scaled mass loss flux hardly vary with changes in the net surface heat fluxes, the values of q_c and q_r can be changed arbitrarily during the iterations to provide updated values of the fuel mass flux, $\dot{m}$. The value for the radiative heat flux is assumed available from the latest solution of the Hottel's thermal radiation equations. The convective heat flux is,

however, a non-linear function of $\dot{m}$ due to the blowing effect of the fuel pyrolysis. This complicates the solution of Eq. (21) for the fuel mass loss rate. A very efficient solution is described in Reference 4 for both horizontal and inclined burning surfaces. The values for the net surface heat fluxes are inputs for determining the mass and the heat release rates of the adjoining flame as follow.

2.2.4   Chemical Heat and Mass Release Rate of Adjoining Flame

Before considering the contribution of a burning surface element to a flame, a set of burning regions adjoining a single flame must be determined. In addition, several such flames need to be determined until all burning regions are accounted for. A practical scheme was developed to organize the construction of multiple flames. The first step was to find a group of nearly horizontal flame spread polygons on which to form pool-like flames. If a nearly horizontal polygon is connected to another flame spread polygon in an adjoining horizontal or vertical panel, then the two flame spread polygons should anchor a single flame. It is possible for a set of such connected polygons to anchor a single flame. Such a flame is described as a merged pool/wall fire. However, if the derived flame height is below the height of a connected vertical polygon, then a separate wall fire is considered for the vertical polygon and the original merged pool/wall fire is no longer anchored to the vertical polygon. After examining all the nearly horizontal polygons for the construction of merged pool/wall fires, all the remaining flame spread polygons will then each have a simulated wall fire.

This organization of multiple flames construction led to two basic flame shapes. The first is the parallelepiped flame shape with the horizontal flame spread polygon as a base for the merged pool/wall fire. The other is the wedged-like shape defined by a boundary layer model for the wall fire. As a consequence, only one additional parameter, the solid flame height, is needed to define the flame shape. It is summarized below.

Cetegen, et al, formula for averaged visible pool fire height is,

$$
z_{f_p}/D =
\begin{cases}
3.3 \left(Q_D^*\right)^{2/3} & ; \quad Q_D^* < 1 \\[2em]
3.3 \left(Q_D^*\right)^{2/5} & ; \quad Q_D^* > 1
\end{cases}
\tag{22}
$$

where

$$Q_D^* = (Q_c/[\rho_a C_p T_a g^{1/2} D^{5/2}]) \qquad (23)$$

Hasemi's formula for averaged visible wall fire height is,

$$z_{f_w}/z_w = \begin{cases} 6.0 \ (Q_w^*)^{4/5} \quad ; \quad Q_w^* < 1 \\ \\ 6.0 \ (Q_w^*)^{2/3} \quad ; \quad Q_w^* > 1 \end{cases} \qquad (24)$$

where

$$Q_w^* = (Q_c/[\rho_a C_p T_a g^{1/2} z_w^{3/2} Y_w]) \qquad (25)$$

Interpolation of flame height for the merged flame is;

$$z_f = z_{f_p} \frac{Q_{c_p}}{Q_c} + z_{f_w} \frac{Q_{c_w}}{Q_c} \qquad , \qquad (26)$$

with a solid flame height:

$$z_{f_r} = 0.4 \ z_f \qquad (27)$$

Both flame shapes have surface elements with their positions, areas and normal vectors defined so that view factors for the thermal radiation model can be numerically calculated among the flames and the mockup surfaces. Once a set of burning surface elements are assigned to a flame, the fuel mass release rate into the flame can be calculated by a summation,

$$\dot{M}_{fuel} = \sum_i (q_c + q_r + q_0)_i \ \dot{m}_i^*(T_i^*) \ A_i \qquad , \qquad (28)$$

and the combustion products mass rate is given by,

$$\dot{M}_j = \sum_i (q_c + q_r + q_0)_i \ \dot{m}_i^*(T_i^*) \ F_j(T_i^*) \ A_i \qquad (29)$$

The chemical heat release rate for the flame is not as straight forward because of the need to account for the incomplete combustion due to the production of soot and carbon monoxide. This is modeled by the equation,

$$Q = \sum_i (q_c + q_r + q_0)_i \left[\dot{h}^* - \dot{m}^* (F_s H_c + F_{co} H_{co}) \right]_{i,T_i^*} A_i \tag{30}$$

where F_{co} is the mass fraction of carbon monoxide as a function of the scaled burn time of the surface element, i, and F_s is the soot mass fraction of fuel calculated from Eqs. (16) to (18) for the flame. The chemical heat release flux of the fuel from a surface element is calculated as the quasi-stoichometric heat release flux minus the heat release flux of the incomplete combustion products of soot and carbon monoxide. The chemical heat release rate of the flame is then the summation of the chemical heat release flux times the area of the burning surface elements. Equation (30) provides a framework for the contribution of each predicted physical processes to the heat release rate of the flame. The virgin surface heating and the flame spread ultimately determines the number of burning surface elements as a function of time and are a major factor in the structure of the thermal radiation field. The scaled burn times of the surface elements directly determine the scaled heat and mass release fluxes and the carbon monoxide mass fractions. The soot specific extinction area and maximum soot absorption coefficient, which are inputs for the soot mass fraction formula, should be treated as functions of the scaled burn time but are constants for the present version of HEMFAST. The flame heat release rate itself determines the flame dimensions, which in turn affects the soot mass fraction (see Eq. (18)) and are also a major factor in the structure of the thermal radiation field. Examination of Eq. (30) also suggest the accelerative growth of the flame heat release rate is due to two main competing factors: the rate of increase of number of burning surface elements and the rate of increase of the surface radiative heat flux. Eventually, a peak value of the flame heat release rate is reached and then its rate of decrease is controlled by the burnouts of the surface elements and the removal of panels.

2.2.5   Thermal Radiation Analysis

The last step in the fixed point iteration scheme is the evaluation of the thermal radiative heat transfer among the mockups, the room, and the gas zones. The thermal radiation analysis is the foundation and also the most complex submodel of HEMFAST. In large fires the thermal radiation dominate nearly all physical processes such that it is worthwhile to have detailed geometrical features and to include coupling effects between thermal radiation sources. Since only a few gas zones and not very many surface elements are considered, the Hottel's zonal model was chosen for the thermal radiation analysis. It was essential to also develop a practical model, because the thermal radiation analysis must be done at each iteration step during each time step. The mean beam length approximations were then applied to the key components of the Hottel's zonal model and the results were reported in Reference 2. One result was to simplify the evaluation of the complex Hottel's exchange areas between the flame and the surfaces to only involve calculations of the configuration factors, surface areas, and the emissivities. An another result was the discovery of a very efficient scheme of solving the thermal radiation equations by taking advantage of energy conservation requirements. Since complex shapes are generated for the flames and for the mockup, the configuration factors were evaluated by numerical integrations. This in turn has made the Hottel's exchange area calculations by far the most time consuming of all the routines in HEMFAST. These calculations, however, are essential for accurately determining the flame spread and the burning rate on the mockup as a function of time.

Thus the input to the thermal radiation analysis are the flame and body structures and properties and the output are the net thermal radiative powers of all gas layers, flames, and surface elements. These output values are fed back into the formulae described in this section for a another iteration step leading to convergence. The output values are also used by the FAST model for the gas dynamics in the room. The coordination of the Furniture Fire Model predictions with that of FAST model predictions is described in the next section on the program structure.

This page intentionally left blank

SECTION 3

PROGRAM STRUCTURE

The structure of the HEMFAST code has undergone evolutionary improvements during the current grant period. The research conducted in the current grant period included: (a) the code restructuring of HEMFAST to enhance the coordination of time integrations between HEMFAST and FFM, (b) the construction of interface subroutines between FAST and the furniture fire modules (FFM) to replace routines inserted in FAST, and (c) the construction of data management of the input database of FFM. The code restructuring was designed to improve HEMFAST model predictions and to make FFM more accessible to other versions of room fire models. These changes were coordinated with CFR personnel.

3.1 COORDINATION OF TIME INTEGRATIONS

In any complex code involving time integration, such as HEMFAST, selection of an appropriate numerical integration scheme to ensure stability, accuracy, and efficiency is very important. Inadequate schemes of numerical time integration can lead to subtle but significant truncation errors not detectable by the user. To get reasonable predictions, the code may be forced to an inordinately small time step that uses too much computer time. Section 2 also discussed other aspects of numerical time integrations that could lead to inaccuracies. The solution of these several problems has resulted in a complete revision of the first version of HEMFAST. The corresponding modifications of FFM algorithms were reported in the Interim Report (Ref. 4) and tested in this reporting period. A close comparison between the time integration schemes of FAST and FFM guided the development of interfacing subroutines.

We note that the influence of the radiative heat flux, from the upper gas layer (before flashover) on the furniture burnrate, is minor compared to the radiative and convective heat flux from the flames to the burning elements. Thus most time integration variables in FAST can be allowed to lag by a time step with respect to the time integration variables in FFM without loss in accuracy or solution stability in FFM predictions. In addition, the time integration variables in FAST are quite responsive to the furniture

burnrate history. These considerations suggest that the FAST modules for time integration should be executed directly after the execution of the Thermal Radiation Analyzer module without an intervening time step. A placement of the FAST modules within the Local Radiative Heat Flux iteration loop was avoided because of the minor effects of FAST predictions on the furniture burnrate and the species production and because of a desired reduction of computer solution complexity and time.

Note that each time-integration variable in FAST is designed to be stable and accurate. Likewise, the integration of the virgin surface element temperatures at least for thermally thin materials in FFM is designed to be well behaved. The formulations of the flame spread rate and of the local heat release rate were designed to be well behaved and are slowly changing functions of time in most situations, so that Euler time integration to estimate the flame front positions and the burn history, respectively, should be acceptable. Ensuring stability and accuracy in the whole solution is most vexing and has proven to be a roadblock to many modelers of room fires or of any other complex physical phenomena. The careful attention given to reconstructing the HEMFAST functional flowchart as shown in Figure 8 was done to minimize problems of this nature.

3.2   CONSTRUCTION OF INTERFACE SUBROUTINES

The first-version routines placed in FAST as a result of incorporating FFM were recoded into interfacing subroutines as a replacement. The interfacing subroutines are kept as few as possible so that minimum changes are introduced into the FAST code itself. One difficulty in constructing the interfacing routines was that certain existing routines in FAST had to be bypassed to take advantage of the full potential of the FFM code. One significant example is the bypassing of FAST thermal radiation modules to utilize the FFM calculation for the thermal radiation field of the room and furniture. The three resulting interfacing subroutines, FFMGO, FFMINT, and FFMOUT are explained in the next three numbered paragraphs.

3.2.1   FFMGO Subroutine

This subroutine solves the furniture fire growth and burnout as a function of time by implementing the HEMFAST functional flowchart shown in

3-2

Figure 8. That is, the modules for surface temperature, ignition, flame spread, and burn history as a function of time are executed. The radiative heat transfer between the fire plume, the gas layers, the mockup surfaces, and the room surfaces using our improved Hottel Radiation Model is also calculated. The subroutine FFMGO was inserted into the subroutine SOLVE of the FAST code. This synchronized the time stepping integration between FAST and FFM in the manner indicated by Figure 8.

3.2.2 FFMINT Subroutine

The variables for input to FAST's calculations of the gas layers and the room surfaces are obtained in the FFMINT subroutine. The values of the variables are calculated from linear interpolation of the FFM predicted parameters as a function of time. Several FAST's subroutines for defining a fire source, called within the SOURCE subroutine, are bypassed to take full advantage of FFM capabilities.

3.2.3 FFMOUT Subroutine

A subroutine (FFMOUT) was inserted into the FAST's output subroutine (RESULT) to print the results of the FFM predictions.

These three interfacing routines and a substantial amount of internal documentation has been incorporated with the second version of HEMFAST. The FFMGO and FFMINT subroutines are the only routines containing common blocks from both FAST and FFM. The FFMOUT subroutine only has the FFM common blocks and none of the FAST common block.

3.3 FFM DATABASE MANAGEMENT

The interfacing subroutines also served the role of managing the bench scale fire data. This permitted a separate approach to reading the FFM database from that in the FAST code. Also it minimized changes to the FAST code and avoided having to learn the FAST database management and emulating it.

The management of the FFM database requires stringing together separate input data files. One input file provides definition of the furniture shape and position; another file provides the complete cone calorimeter database for different materials; and yet another provides user input for ignition source

and for control of spatial/temporal resolutions. This data management required development of a short menu in the current version so that the user can select the different input data files for stringing together.

3.3.1   HEMFAST Main Program Routine

This main driver routine manages the FAST and FFM input database through a user interactive menu and calls the fire growth algorithms. The structure is described in Figure 10. HEMFAST is designed to default to the FAST model if other fire sources other than furniture fire are specified in the FAST input data. In that case, HEMFAST will not ask for the FFM input data from the computer files. On the other hand, if the furniture fire source is specified by FAST input, the user interactive menu reads in the huge FFM database files in the following order: mockup geometry constructor file, thermal properties and flame spread data file, and the cone calorimeter data files corresponding to different external irradiances.

The user interactive menu then implements the FFM bench scale processor subroutines described in Figure 2 to process the FFM basic database. Only the processor routine for the cone calorimeter database is currently incorporated into HEMFAST. Reference 4 documents the good progress made in this area. The processor routine for the flame spread database is not incorporated in HEMFAST. That is, no improvement was achieved beyond the flame spread data processing described in Reference 2. The menu next executes the FAST and FFM fire growth subroutines, which includes the interfacing subroutines. As a note, a modeler only needs to understand the routines HEMFAST, FFMGO, FFMINT, and FFMOUT to implement FFM into updated versions of FAST (or even the Harvard CFC).
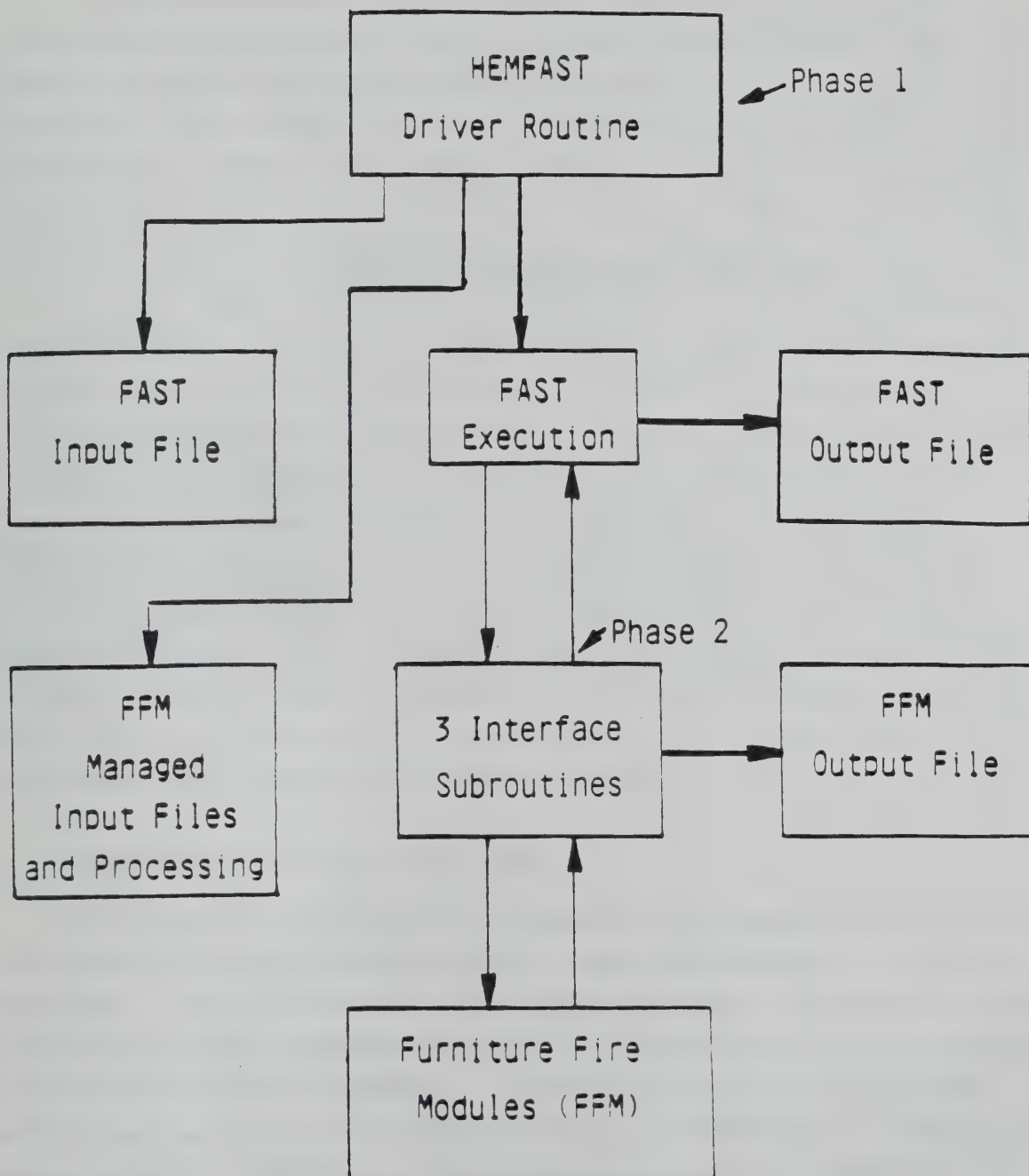
Figure 10.   Revised code structure of second version of HEMFAST

This page intentionally left blank

MODEL VALIDATION

The revision of the time integration algorithms in FFM and its synchronization with the FAST time integration has been tested. The results show a much improved solution stability and efficiency over the first version of HEMFAST. This was made possible by incorporating quasi-stable explicit predictors for the furniture surface temperatures, for the flame spreading fronts and for the furniture element burn histories. The stability of the solution was also assisted by coupling the combustive heat and mass release rates with the flame convective and radiative heat fluxes in a convergent iterative scheme. The improved stability in the solution allowed greater variation to be taken in the time steps and furniture element sizes.

The predictability of the FFM code is further demonstrated by the effect that the mockup geometry has on the dynamic fire variables. For example, the flame spread is allowed to proceed in any direction on the mockup and the flame spread velocities also vary with surface orientation and with other physically based variables. This flame spread behavior also results in a dynamically changing flame volume and shape. The current version of HEMFAST is thus suitable for model validation with selected fire tests. Full and bench scale fire tests needed to be examined first to assure compatibility and completeness for input to FFM processing routines.

4.1 SELECTION OF FULL SCALE FIRE TESTS

We have acquired the furniture/room fire tests database from Dr. Vito Babrauskas, Mr. Richard Peacock, and Dr. James Quintiere while at NBS in August 1987. This database has been examined to select individual fire test results and to select measured variables for comparisons with the predictions of the second version of HEMFAST. In particular, mockup burning rates, burning regions and the combustion products are compared as a function of time between model and experiment. The results are discussed in Section 4.2.

The full scale fire tests were selected on the basis of compatibility with our current processed bench scale data as well as on the basis of the thoroughness of full scale fire test measurements and documentation. The results of the full scale fire tests were reported in Refs. 14 to 19 and some

of the data were acquired in the form of data sheets, VCR observations, or data plots. Examination of these data suggested grouping of the database into three validation levels, as shown in Table 1.

4.1.1   Fire Test Data - Level A

The top group level, A, seemed to provide best thoroughness and compatibility between the full scale fire test and the bench scale tests. The group A database has four-cushion, fabric/polyurethane, chair mockups tested both in the furniture calorimeter (Ref. 14 & 15) and in the full scale room fires (Ref. 18). These databases are the most thorough because they included VCR observations of mockup fire growth, the complete furniture calorimeter data logging (and logged into our VAX disk files), and a most recent detailed room fire measurements (reported in Ref. 18). The simple four-cushion chair construction with ignition on the seat is most easily simulated by the HEMFAST code. Lastly, the same fabric/foam materials were tested in the cone calorimeter and on the horizontal flame spread apparatus. The scaling constant q_o, c, and d in Eqs. (9) and (13) as well as the thermal ignition parameters were effectively determined by considering similar materials tested fully in the bench scale experiments. Eventually, the issue of full compatibility between the full scale tests and the bench scale tests will be addressed.

4.1.2   Fire Test Data - Level B

The data at the B level include realistic furniture constructions. They do not seem to be as thorough and compatible as the A level database. Although the furniture calorimeter and the room fire tests are complete, the realistic construction of furniture provides a challenge to HEMFAST's furniture fire modeling due to approximating the furniture geometry, to igniting the furniture by a simulated wastebasket fire, and to a more severe extrapolation of the cone calorimeter data to varying foam thicknesses of the furniture. The bench scale data for Group B mockups are somewhat more complete than that of Group A mockups because cone calorimeter data exist for four cone irradiance levels for all materials and the thermal ignition data exists as well. But the flame spread data are based on bench scale tests with similar materials. Once again the full compatibility of various databases is an issue to be resolved with future modifications of the database.

Table 1

SELECTION AND ORGANIZATION OF FULL AND BENCH SCALE TESTS

Group Number	Mockup Configuration	Foam/Fabric (Notation in Ref 14)	Furniture Calorimeter Data	Full Scale Tests	Cone Calorimeter Data[14] (Cone Radiance in kW/m²)	Flame Spread Data	Thermal Ignition Data
A.1	4-Cushion Chair	FR PU/HC	Test#17 in Ref 14,15	Ref 18	25	Mockup fire growth on VCR. Bench scale data in Ref 14 and processed in Ref 2	Similar to materials in Ref 14 and processed in Ref 2
A.2	4-Cushion Chair	NFR PU/LO	Test#12 in Ref 14,15	--	25		
A.3	4-Cushion Chair	FR PU/BO	Test#14 in Ref 14,15	--	25		
B.1	Chair-F21	FR PU/LO	T19 in Ref 14,16,17	T45 in Ref 17	25,30,40,50	Similar to materials in Ref 14 and processed in Ref 2	Bench scale data in Ref 14 and processed in Ref 2
B.2	Loveseat-F31	FR PU/LO	T31 in Ref 14,16,17	T37 in Ref 17	"		
B.3	Sofa-F32	FR PU/LO	---	T38 in Ref 17	"		
B.4	Chair-F24	FR PU/HC	T22 in Ref 14,16,17	-	"		
B.5	Chair-F25	NFR PU/LO	T29 in Ref 14,16,17	-	"		
C.1	4-Cushion Chair	FR PU/-	Test#28 in Ref 14,15	-	25	Bench scale data in Ref 14 or 20 and processed in Ref 2	Bench scale data in Ref 20 and processed in Ref 2
C.2	4-Cushion Chair	NFR PU/-	Test#29 in Ref 14,15	-	25		
C.3	Horizontal Pod	Cellular Plastic#32	-	Ref 19	Similar to NFR PU		

1 Data sheets acquired from cone calorimeter tests in NBS-CFR facility and corresponding processed data reported in FY 1987 progress reports (see Ref 4).

4.1.3   Fire Test Data - Level C

The C level databases as listed in Table 1 were selected mainly to demonstrate flexibility of the HEMFAST model in the case where the compatibility between the full scale tests and the bench scale tests is barely acceptable. The polyurethane foam without fabric used in the mockups for full scale tests (in Refs. 15 & 19) is supposed to be similar to the foams tested at bench scale level (in Refs. 14 or 20), and cone calorimeter data for a different similar foam at a single cone irradiance value are all that is available.

The furniture calorimeter tests listed in Table 1 provide measurements of the mockup heat and mass release rates, the production of combustion gases, and of the soot extinction area and mass fraction as a function of time. The large scale tests also provide temperature measurements of the upper and lower gas layers whereas the fire products or wall temperatures are measured only occasionally. The most reliable variables for validation with the furniture calorimeter are the heat and mass release rates and the soot extinction areas as function of time. The techniques for sampling and measuring gases concentration and soot mass in the furniture calorimeter were still incorrect at the time the measurements were made for the tests listed in Table 1.

4.2   VALIDATION WITH FURNITURE CALORIMETER FIRE TESTS - LEVEL A

The most important model validations are with the Level A database because of the following features. The VCR observations show the burn areas, the occurrence of thermal ignitions, and a complex flame shape as a function of time. The furniture calorimeter associated with this database provides reliable values of the mockup heat and mass release rates as a function of time and of some soot extinction areas. The samplings of soot and of combustion products were not yet reliable nor available. The bench scale database is fairly thorough as explained previously.

As listed in Table 1 under Level A, the four cushion mockup with three different cushion types provided a good challenge to the predictability of the HEMFAST model. That is, the VCR observations show an initial accelerative horizontal flame spreading, some flame spreading to the back cushion, and then thermal ignitions of the remaining cushion areas at a critical time. Three

cushion composite types were selected; heavy olefin fabric/fire retarded polyurethane foam, light olefin fabric/non fire retarded polyurethane foam, and heavy cotton fabric/fire retarded polyurethane foam. These cushion types provided a challenging range of values for the flame spread rates, for the heat and mass release rates, and for the soot extinction areas.

The FFMGO and FFMOUT subroutines contain routines for storing the model predictions in the various files as a function of time. The fire test data of the corresponding variables are also stored in similar files. These data files are accessed by two plotting programs. One provides three-dimensional graphics of the flame spread polygons on the mockup and the other program plots the model predictions versus the fire test data as a function of time.

4.2.1   Results With 4-Cushion Mockup, HO/FRPU Material

The predicted snapshots of the flame spread on the 4 HO/FRPU cushion mockup at every 20 seconds are shown in Figure 11. The piloted ignition point is located in the middle, 100 mm from the back cushion. The actual mockup has cushions with the length and width as 0.61 m and the thickness as 0.1 m. The simulated cushions have slightly larger lengths and widths to translate the burning areas of the edges of the actual cushion onto a panel surface. The horizontal flame spread in the figure initially proceed at the minimum rate and then accelerates as the virgin material surface is preheated by the radiating fire plume. The flame spreading on the back cushion is a result of rapid upward flame spread once the horizontal flame spread reaches the back cushion. The resulting merged pool/wall flame develops a more intense radiative heating of the surfaces so that thermal ignitions and separate wall fires occur on the left and right cushions. By this time the flame spreading is almost instantaneous and a single merged pool/wall fire is established on the mockup. Each and every flame spread polygon, which by now completely covers the adjoining panel, begins to recede into the cushion thickness. The slight non-symmetry of flame spreading in the accelerated phase is probably due to the error tolerance in the iteration solution of the radiation balance equations. Symmetries were not built into the model because general mockup constructions and alternate locations of piloted ignition are the features of the model.
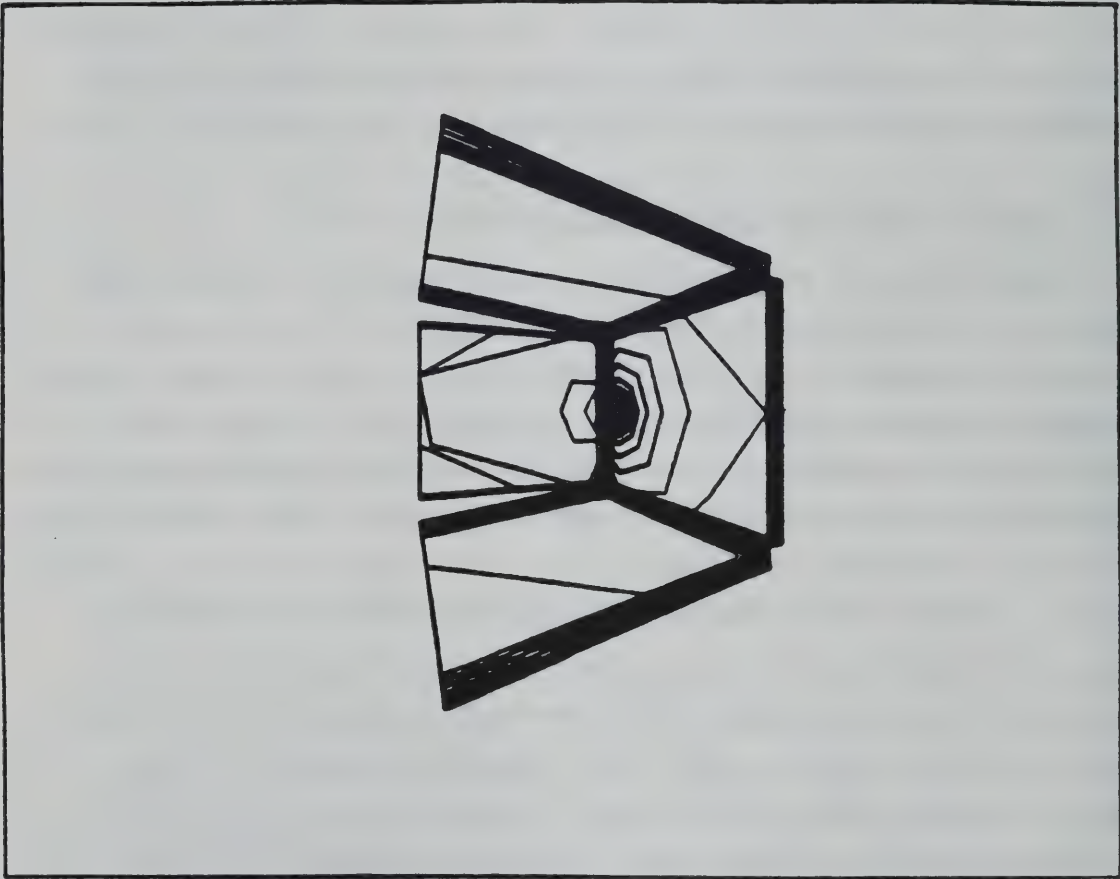
Figure 11. Furniture fire spread on HO/FRPU material

The comparison of the flame spreading to the fire test data, however, is based on the fractional burn area of a cushion as a function of time. Since each cushion was marked into 10 cm by 10 cm surface elements, the VCR observations were used to count the number of burning elements. This information was converted into the fractional burn areas. The derived data is represented by the symbol data points in Figure 12. It is recalled from section 2.1.1 that the parameter corresponding to the conductive heat flux from the anchored diffusion flame, i.e., the product of Eqs. (6) and (7), needed calibration for a given material.

The calibration obtained in Reference 2 from the measurements with the horizontal flame spread apparatus for the given material was found to be inadequate. That is, the preheated surface temperature, T_e, as defined in Reference 2 did not include preheating by the fire plume radiation. Instead, the effect of the fire plume radiation was lumped together with the conductive heat transfer of the anchored flame to define a constant for the summation term in Eq. (4). This constant, however, can be used to provide an initial high value for the product, $q_f \delta_f$, during a calibration process that uses the HEMFAST code itself. The HEMFAST code currently does not have the feature of the flame spreading from a line ignition source in order to calibrate with the horizontal flame spread apparatus. This can be easily be resolved when the next version of HEMFAST is created. The data for the horizontal flame spread froma point source, that can be used to calibrate $q_f \delta_f$ for now, are the circled symbols in Figure 12. The result of the calibration is $q_f \delta_f = 0.2$ KW/m, which is two thirds of the corresponding summation constant in Reference 2. The application of the two thirds factor for the other fabric/foam materials was also successful in calibrating $q_f \delta_f$ for those materials. Thus there is still promise in using the data from the flame spread apparatus as a basis for calibrating flame spread constants.

The solid curve in Figure 12 is then the calibrated curve versus the circled data for the mockup seat. If the fire plume radiation was not a contribution to the flame spread rate, then the solid curve would have been approximately straight instead of a exponential-like shape. The dash line for the rear cushion in Figure 12 corresponds to the upward flame spread behavior in fair agreement with the data. The remaining dash lines for the left and right cushions show a very rapid rise due to both the upward flame spread and
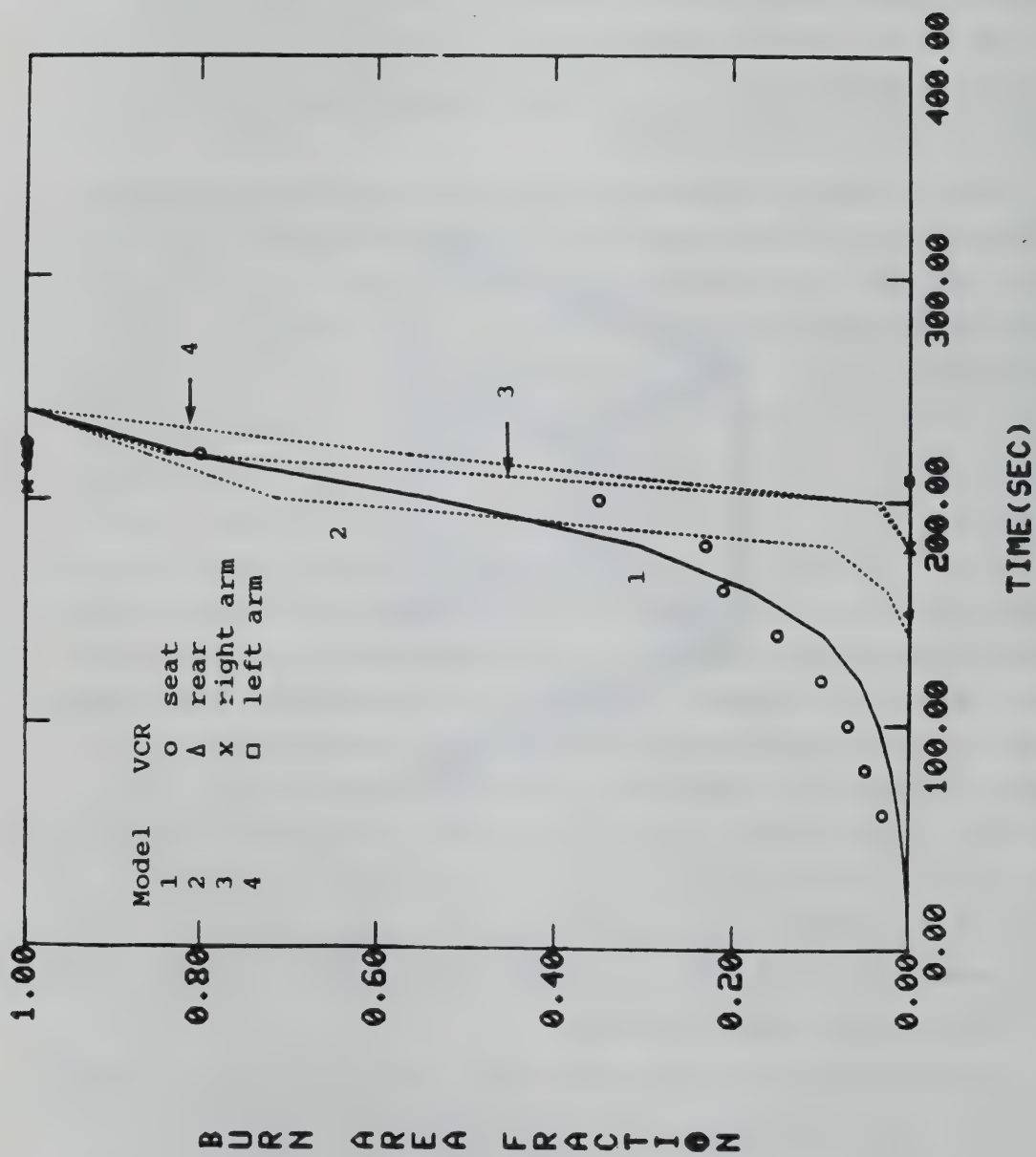
Figure 12. Burn areas comparison for HO/FRPU material

the thermal ignitions of the remaining virgin elements. The results conclusively demonstrate the combined formulation of the flame spread with radiative heating and of the thermal ignitions of virgin elements are essential to the prediction of the furniture fire growth.

The most important model validation is the comparison of predicted burnrate of the fire versus that measured in the furniture calorimeter. This is shown in Figure 13. The rapid rise in the burnrate at around 200 seconds coincides with the very rapid rise in the burn areas. The peak burn rate at about 250 seconds is in good agreement with the fire test data. The drop in the burnrate at about 300 seconds is due to the burnout of some burning elements. The predicted burnrate curve drops below the data points in the remaining part of the time because the burning on the outside surfaces of the mockup were not simulated. Fairly large time steps of 20 seconds demonstrate the effectiveness of the new time integration schemes.

The prediction of the furniture mass loss rate versus the data in Figure 14 shows features similar to the burnrate comparisons, although the agreement is not quite as good. Figure 15 presents the HEMFAST predictions of the soot extinction area as a function of time versus the furniture calorimeter reported value near the peak burnrate. The agreement is quite good during the significant fire growth stage from 150 to 250 seconds. Since the burnout phase beyond 250 seconds admittedly needed better simulation, the solid curve after 250 seconds in Figure 15 is inconclusive. It would be interesting to see if similar agreements of the soot extinction areas are obtained with other materials, as there are no calibrating constants involved in the soot quantity predictions.

In retrospect, the validation of the FFM portion of HEMFAST requires, as the minimum, the comparisons with the surface burn-area data, the furniture burnrate data, and the soot extinction area data as a function of time. The main reason is to sort out the high degree of coupling between the physical processes of flame spread, the burnrate, and the soot production.

Other predictions of HEMFAST are presented in Figures 16 to 18 without any corresponding fire test data. Figure 16 is the predicted convective heating rate summed over all elements of the mockup. The values are typically much smaller than the burnrate of the furniture fire. The
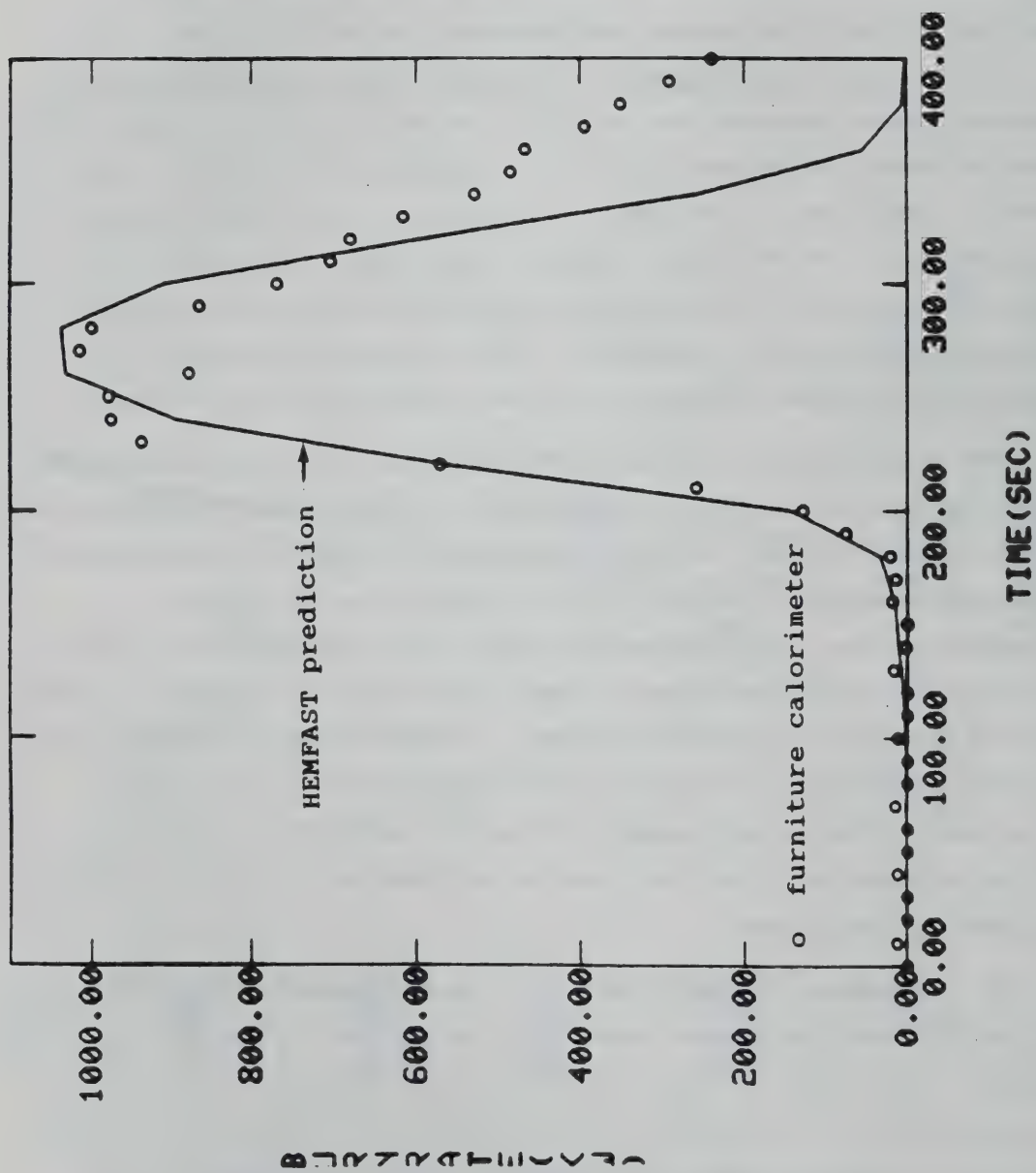
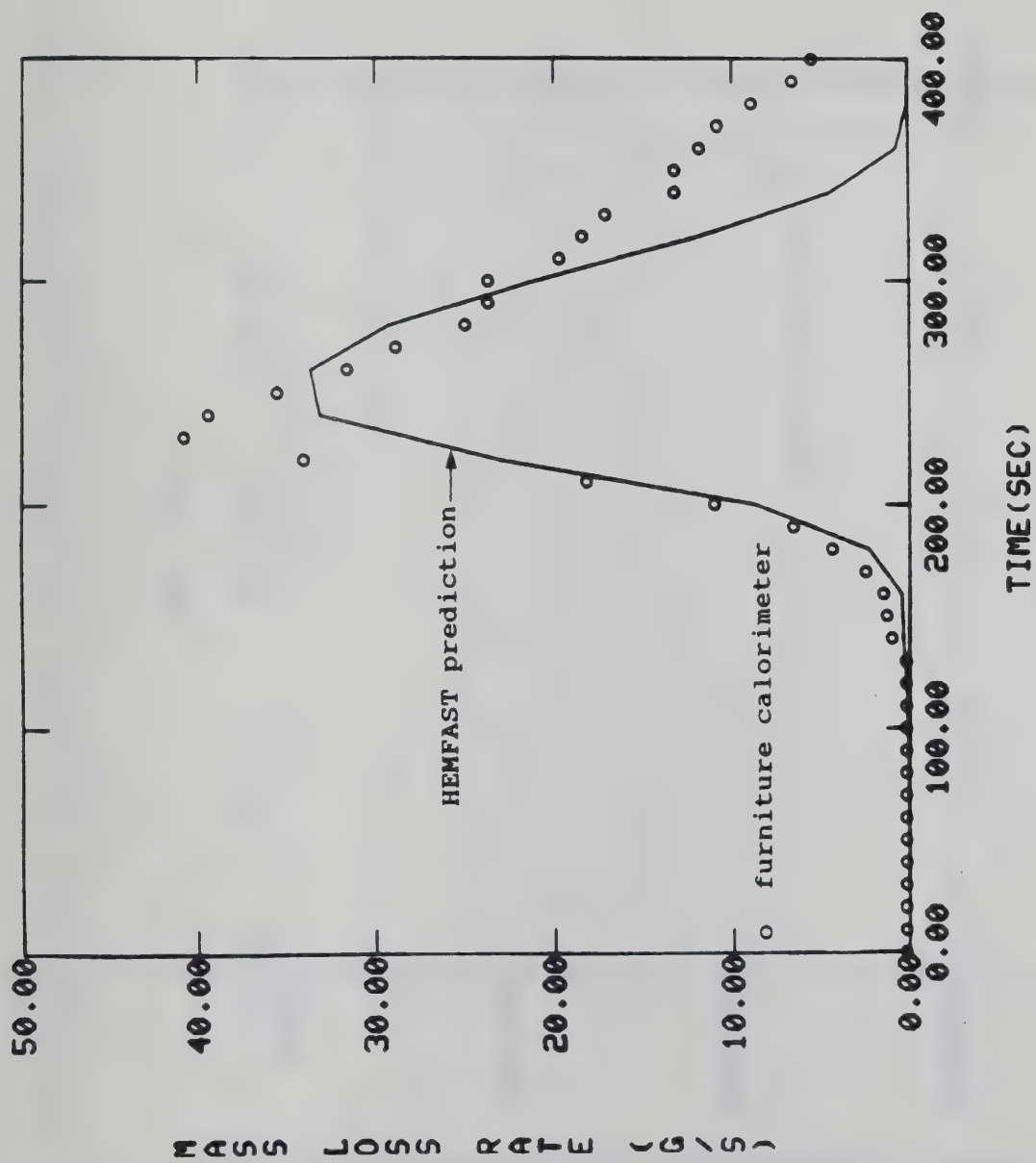Figure 13. Heat release rate comparison for HO/FRPU material

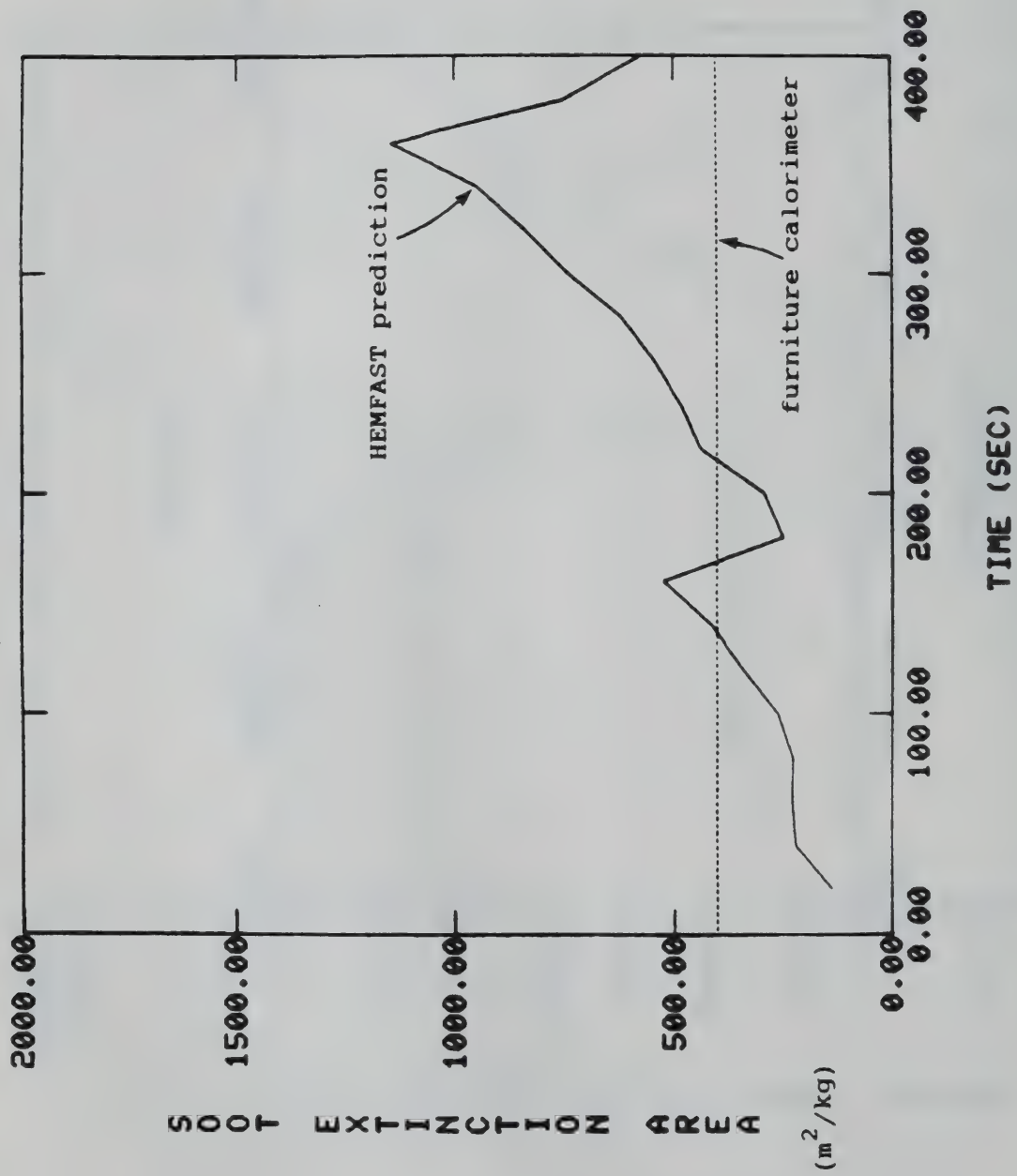Figure 14. Mass loss rate comparison for HO/FRPU material

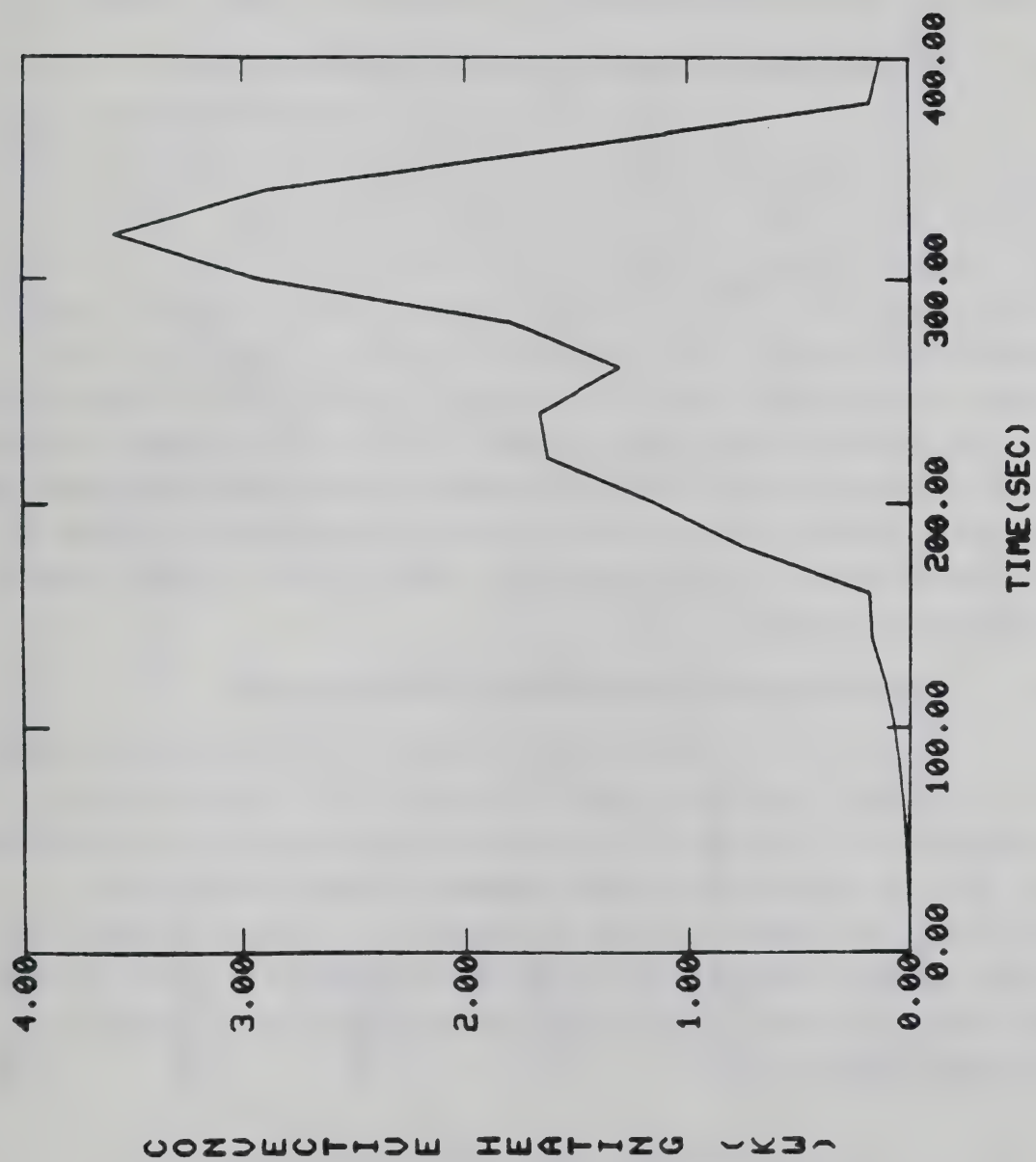Figure 15. Soot extinction area comparison for HO/FRPU material

Figure 16.   Convective heating of mock up for HO/FRPU material

predictions associated with the FAST program are shown in Figure 17. The predicted temperatures of upper and lower gas, upper ceiling, the walls, and the floor are shown as a function of time. Further variations in the input to FAST is needed to reduce the inconsistency between the upper and the lower gas layer temperatures. Finally, the combustion product mass fractions of O_2, CO_2, H_2O, CO, HCl, and HC are presented as a function of time in Figure 18.

4.2.2 Results With 4-Cushion Mockup, LO/NFRPU Material

Figures 19 to 23 provide plots for the LO/NFRPU material similar to Figures 11 to 15. The time steps of 10 seconds are used instead of 20 seconds because of the rapid flame spreading near 100 seconds as shown in Figure 20. The conclusions relating to the results in the figures are similar to the previous section. The only exception is a possible numerical problem at 130 seconds in Figure 21 whose resolution may shift the location of the peak burnrate closer to the data. In any case, the peak value of the burnrate agrees with the fire test data value of about 1500 KW. We note that the peak burnrate and the mass loss rate of LO/NFRPU material are about 50% higher than that of HO/FRPU material, but the soot extinction area tends to be about 50% less. The HEMFAST model is thus capable of predicting these changes between the two different materials.

4.2.3 Results With 4-Cushion Mockup, HC/FRPU Material

The Heavy Cotton fabric/Fire Retarded PolyUrethane foam material is difficult to ignite and flame spread and provides low burnrate output. Even so, the results in Figures 24 to 28 indicate somewhat similar conclusions as above. The time step was 40 seconds because the rapid flame spread occurred at about 400 seconds as shown in Figure 25. The peak burnrate has dropped down to about 500 KW, as also predicted by HEMFAST, but the soot extinction area show greater fluctuations averaging around 300 m*m/Kg in poorer agreement with the data.
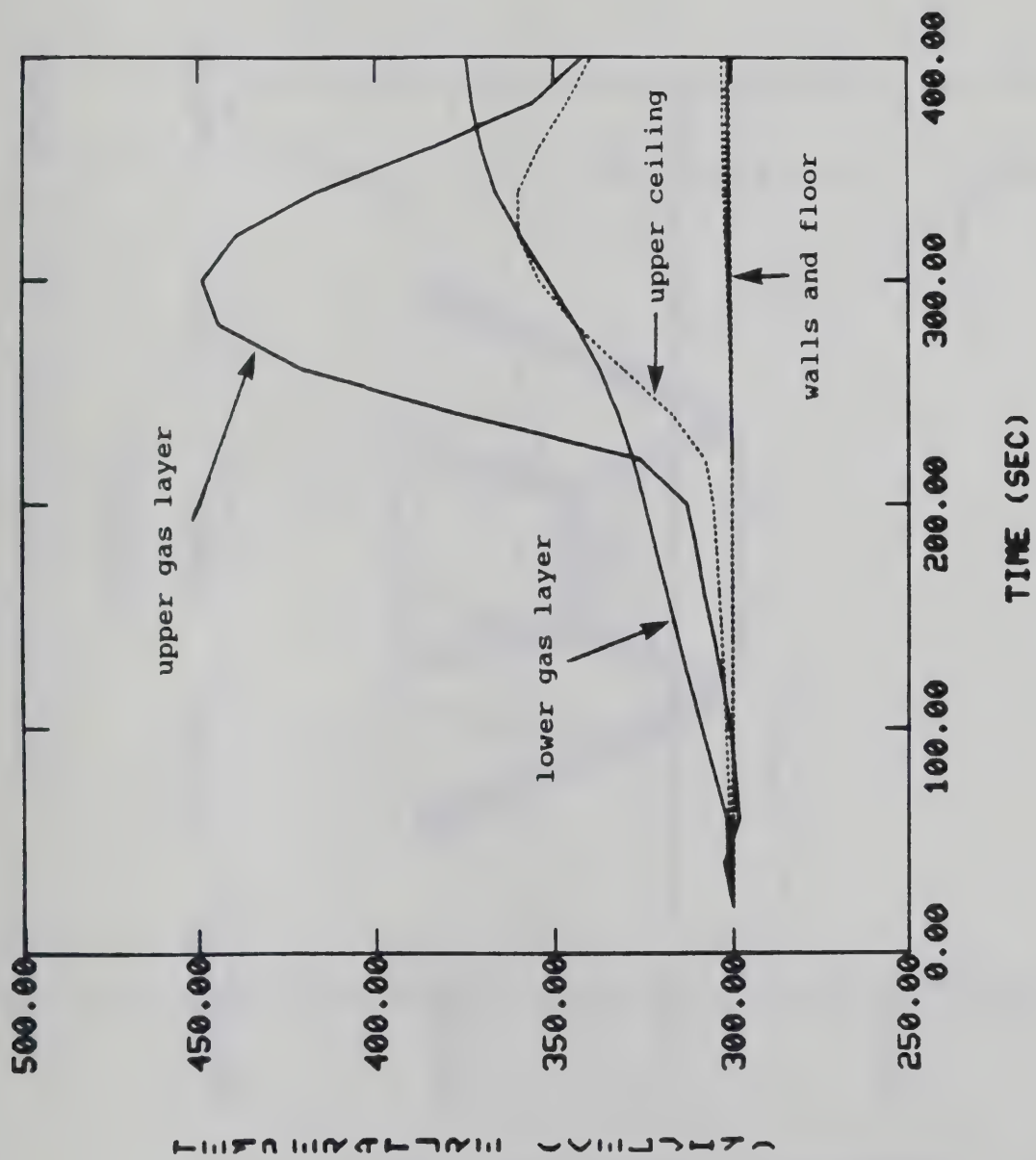
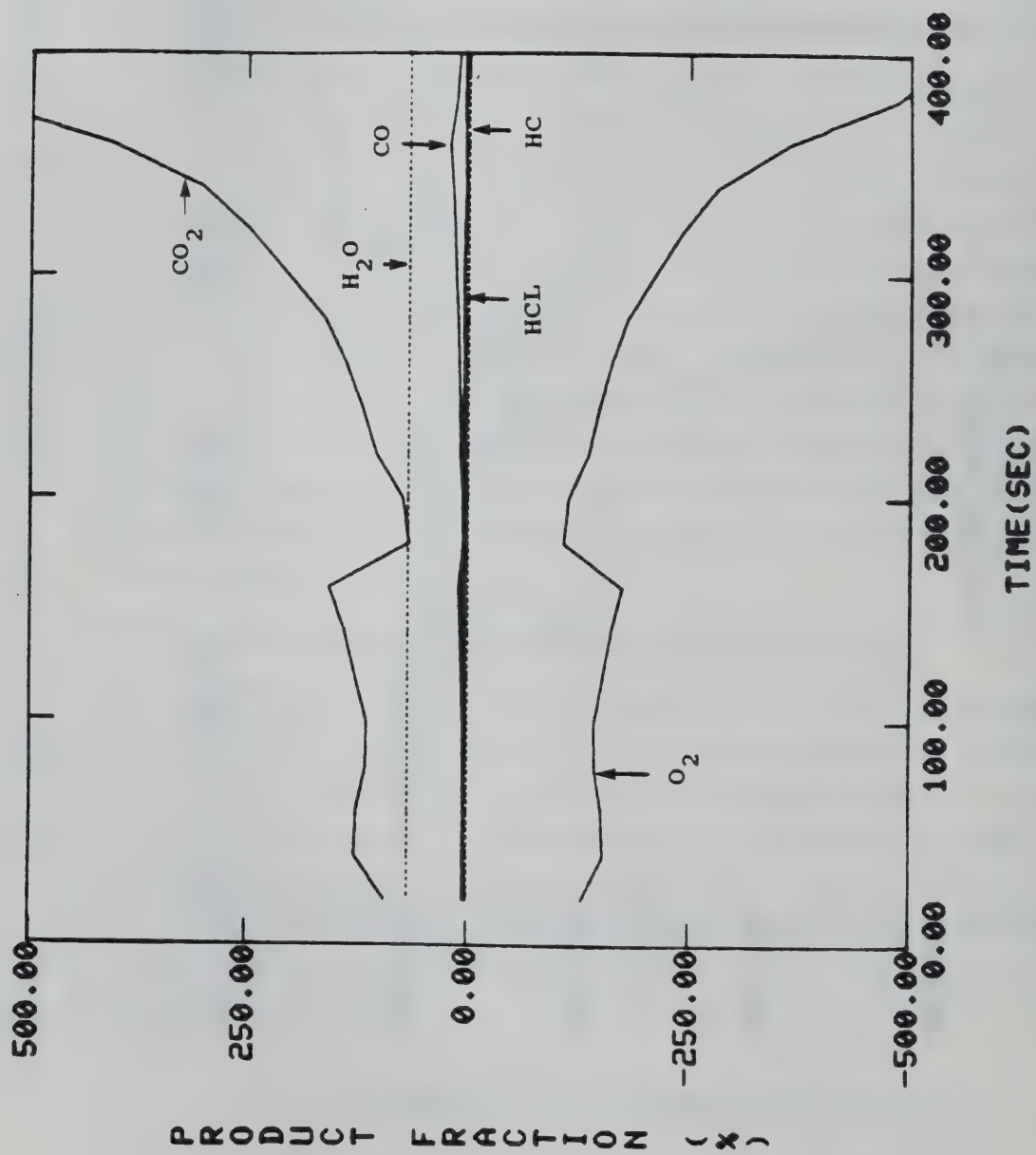Figure 17. Gas and wall temperatures predictions of HEMFAST
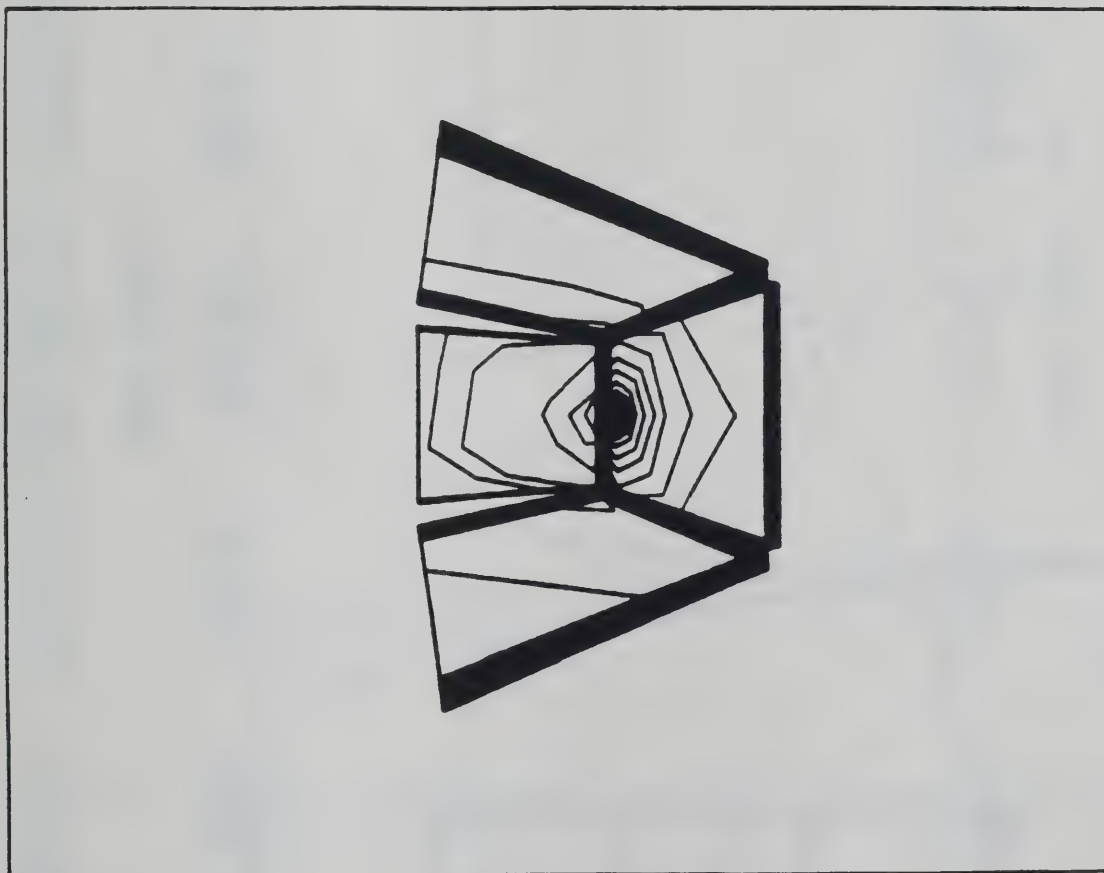
Figure 18.   Combustion product predictions of HEMFAST

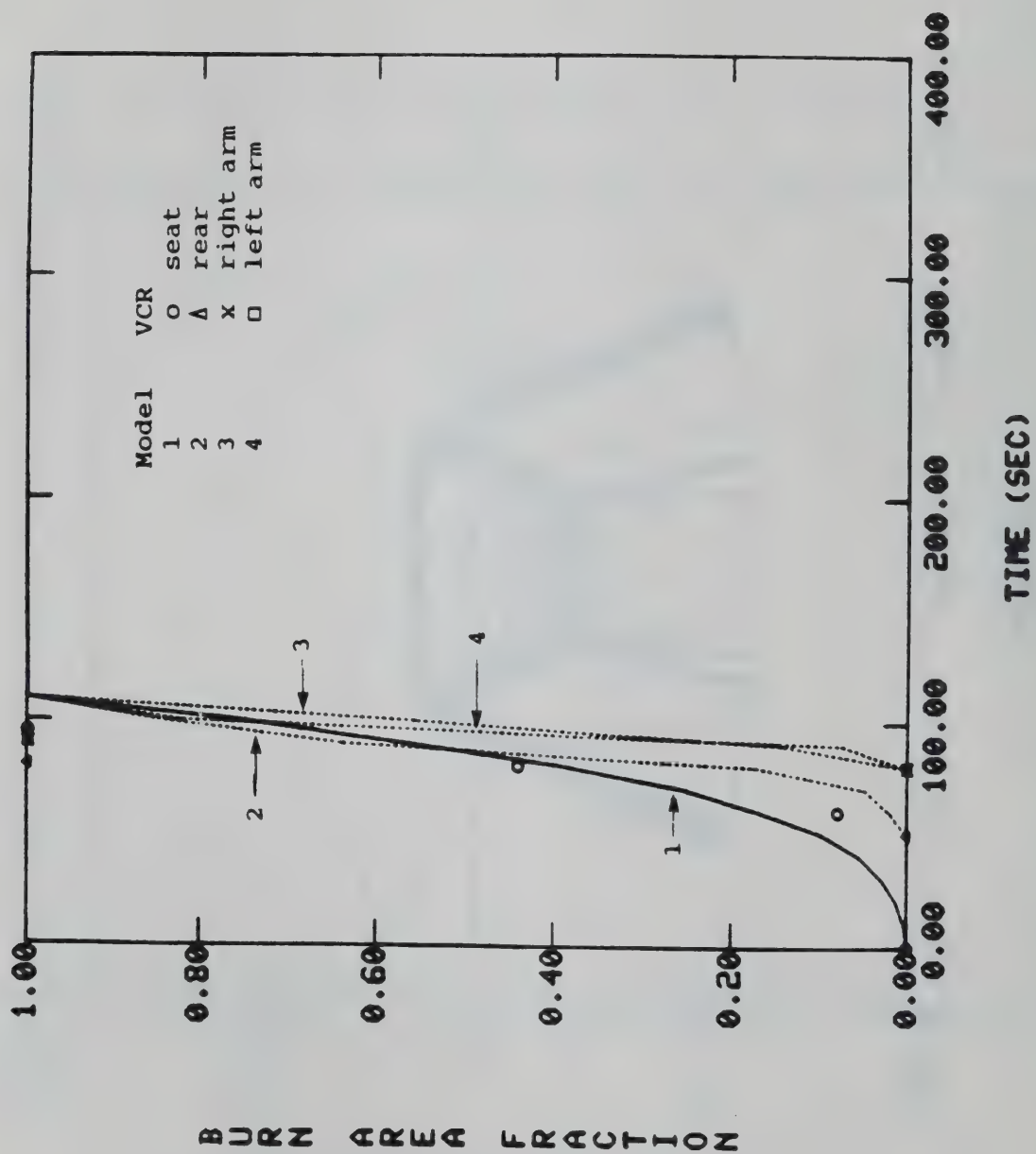Figure 19. Furniture fire spread for LO/NFRPU material

4-17

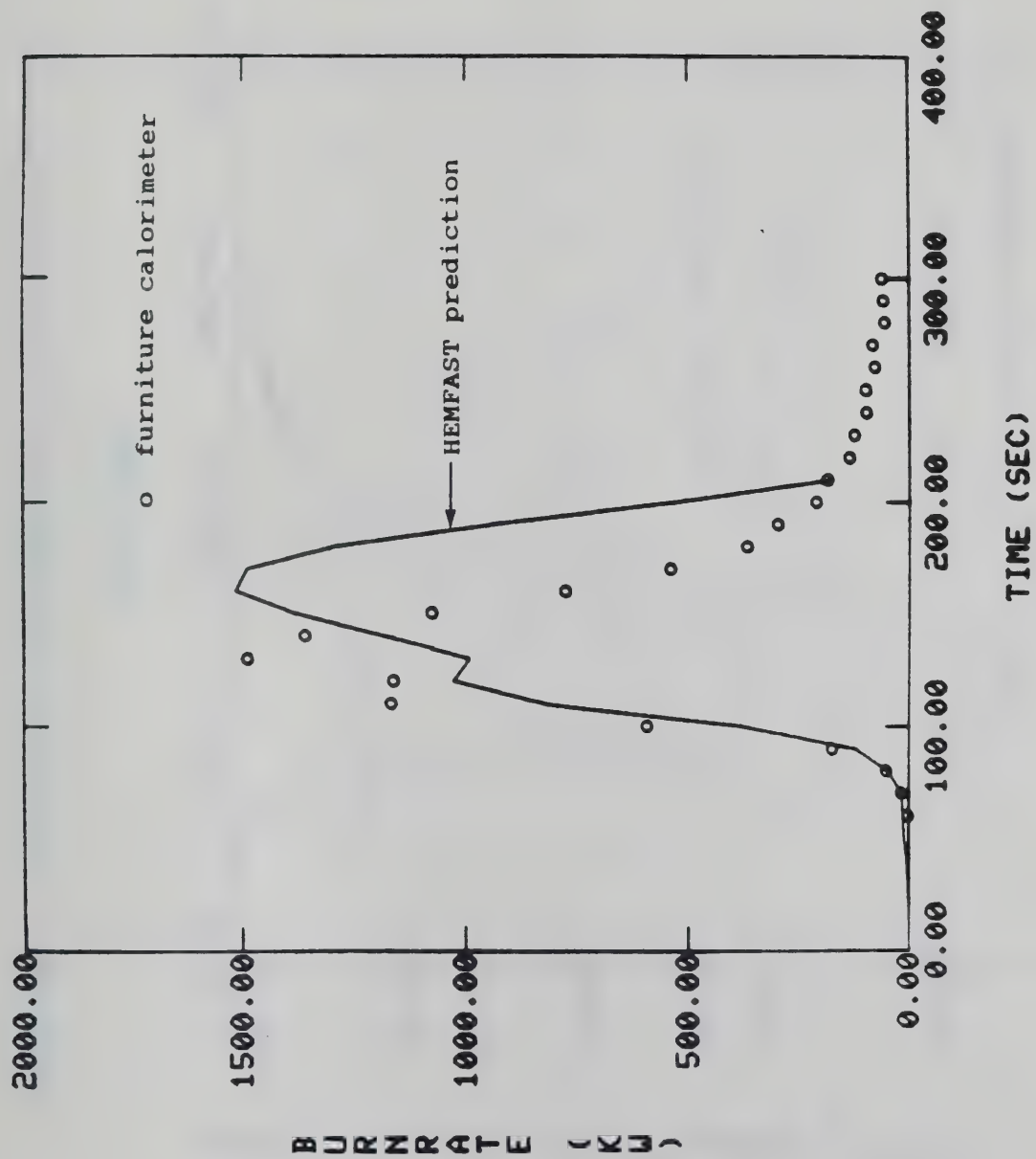Figure 20.   Burn areas comparison for LO/NFRPU material

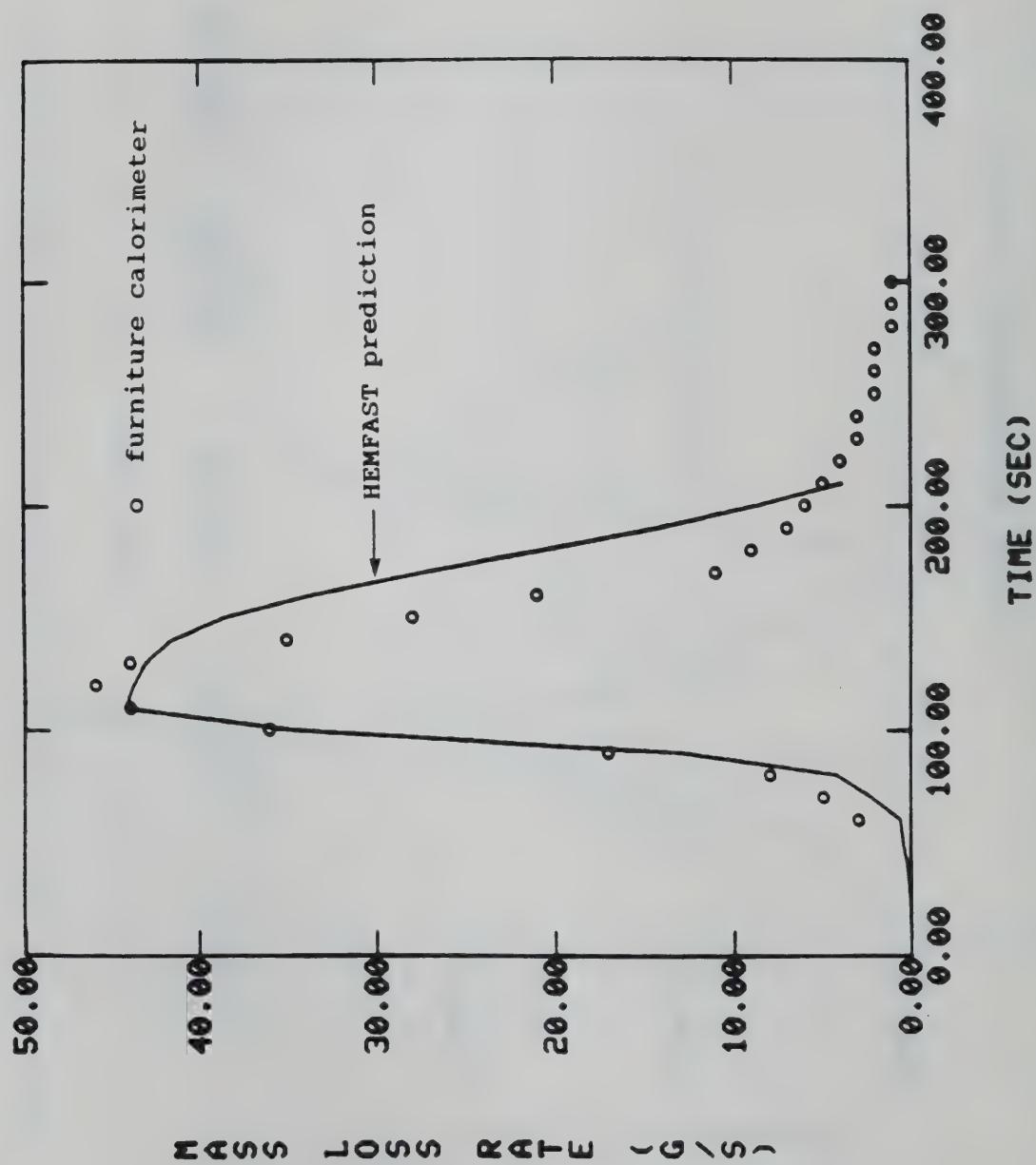Figure 21. Heat release rate comparison for LO/NFRPU material

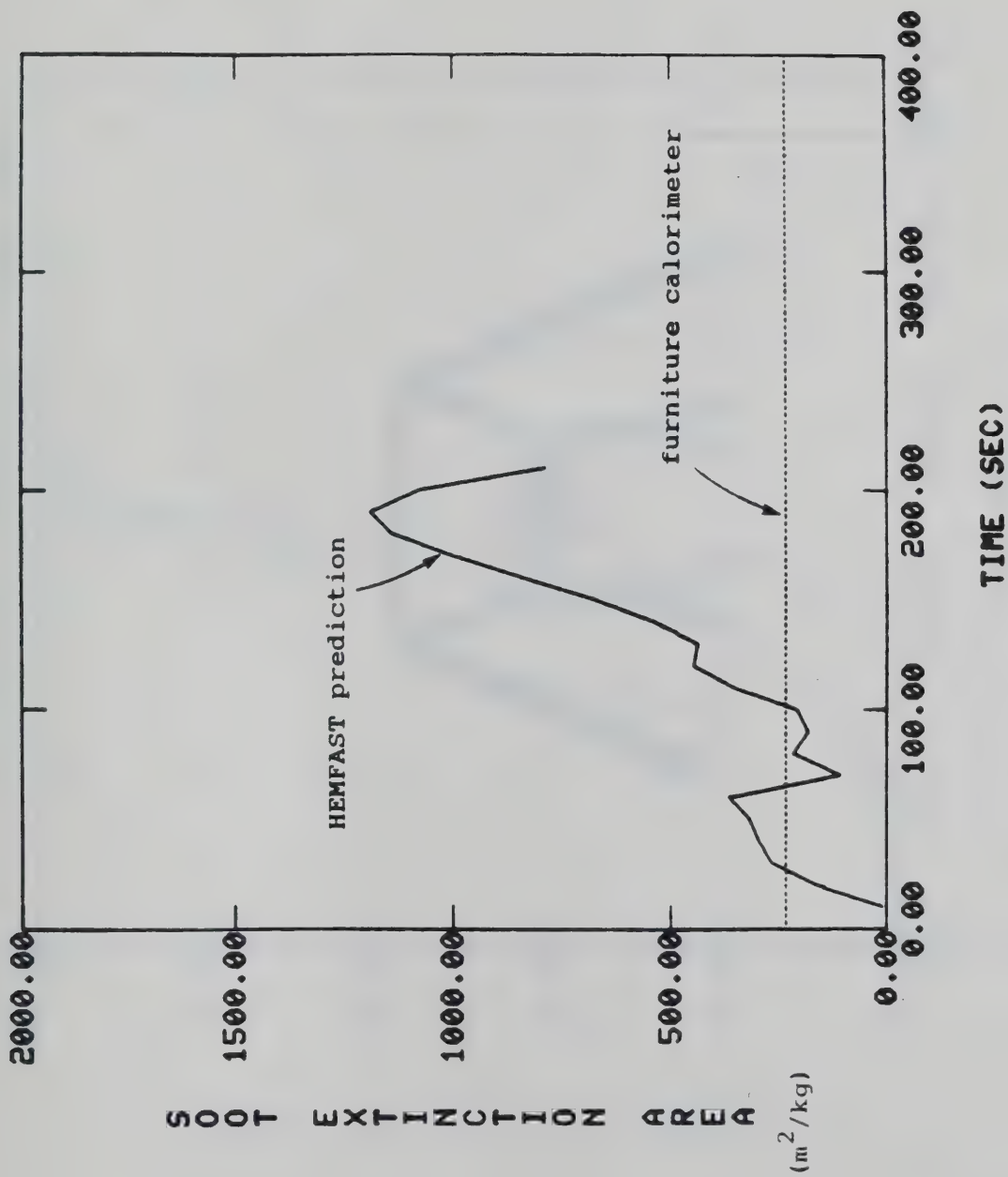Figure 22. Mass loss rate comparison for LO/NFRPU material

Figure 23. Soot extinction area comparison for LO/NFRPU material
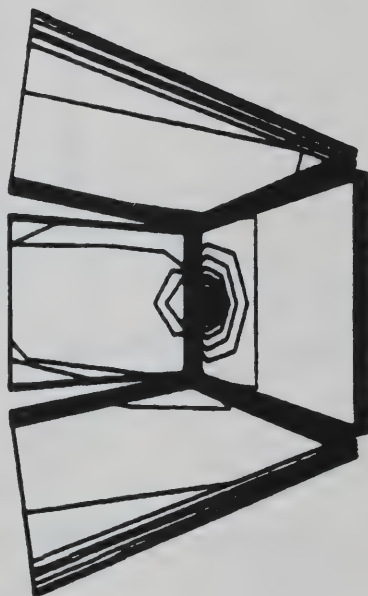
4-21

4-22

C1. FURNITURE FIRE SPREAD

Figure 24. Furniture fire spread for HC/FRPU material
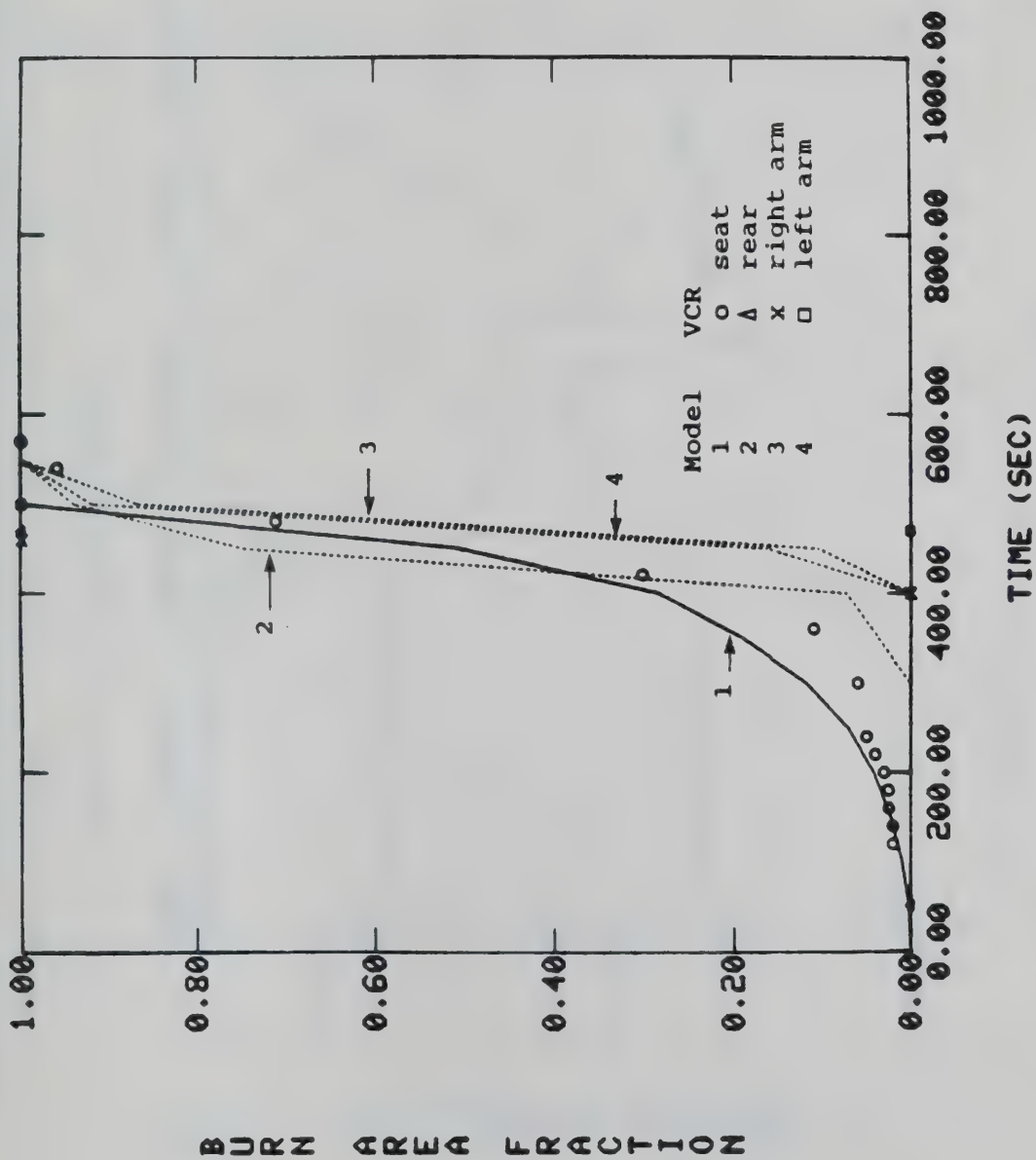
Figure 25. Burn areas comparison for HC/FRPU material
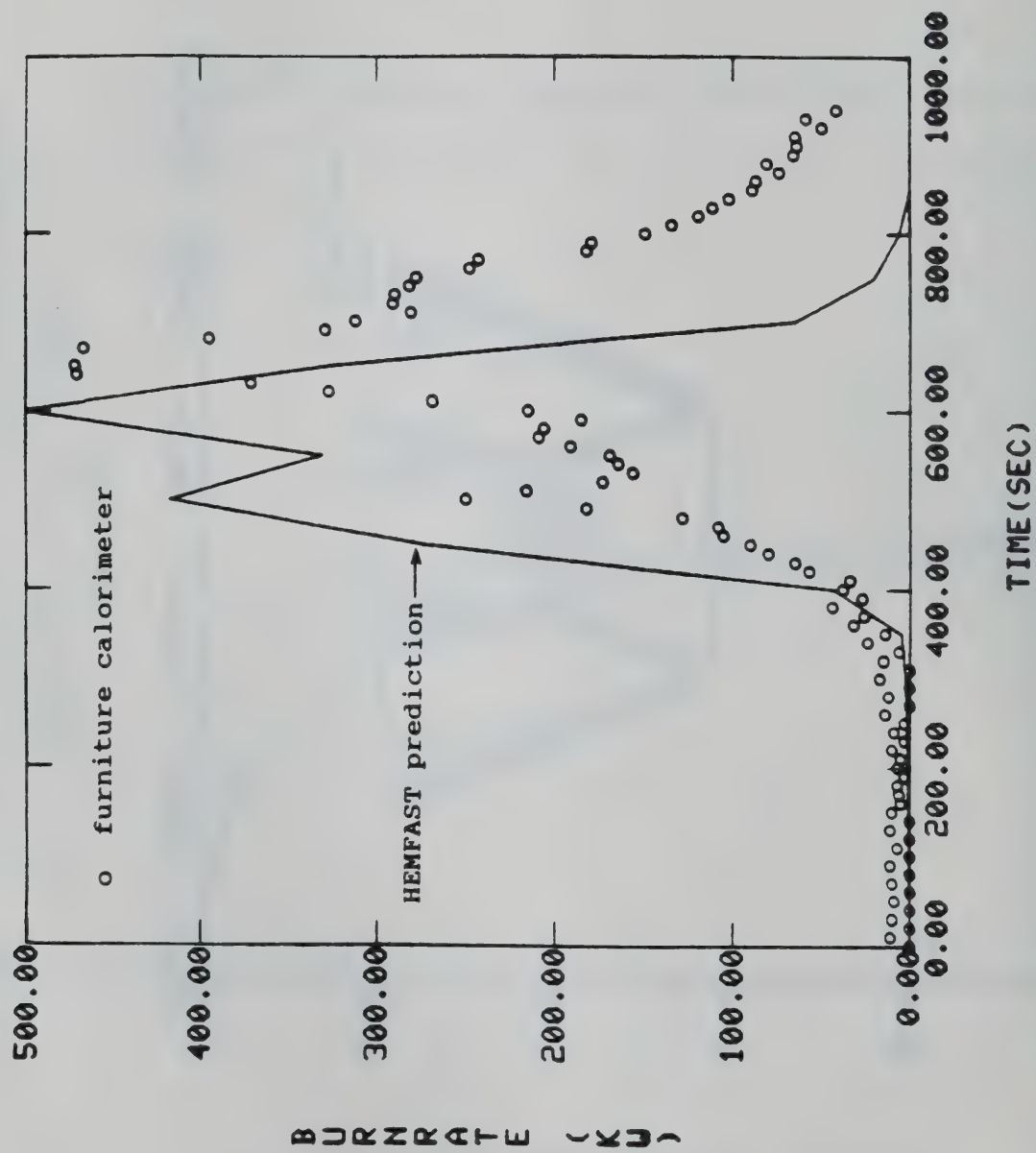
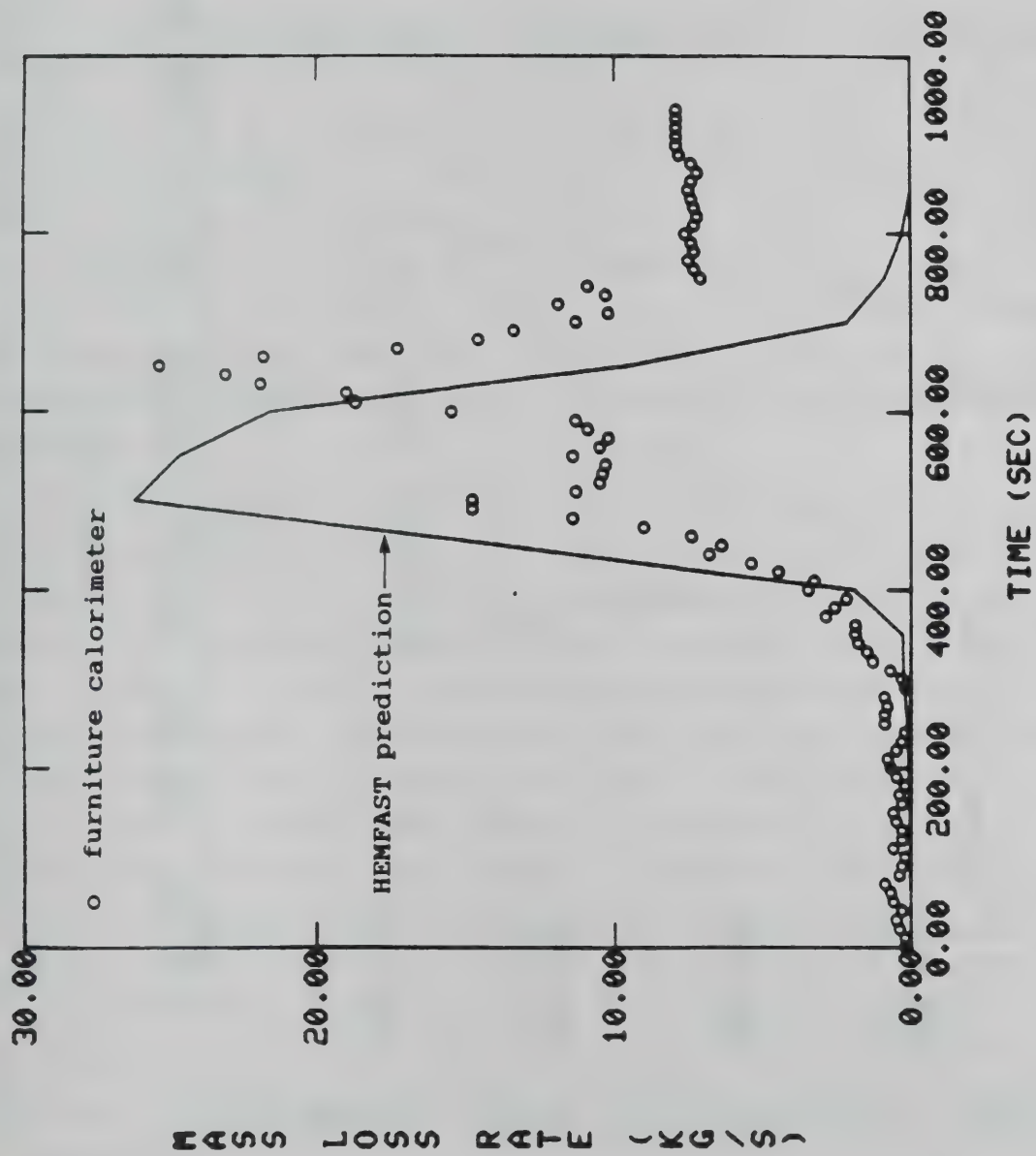Figure 26. Heat release rate comparison for HC/FRPU material

4-24

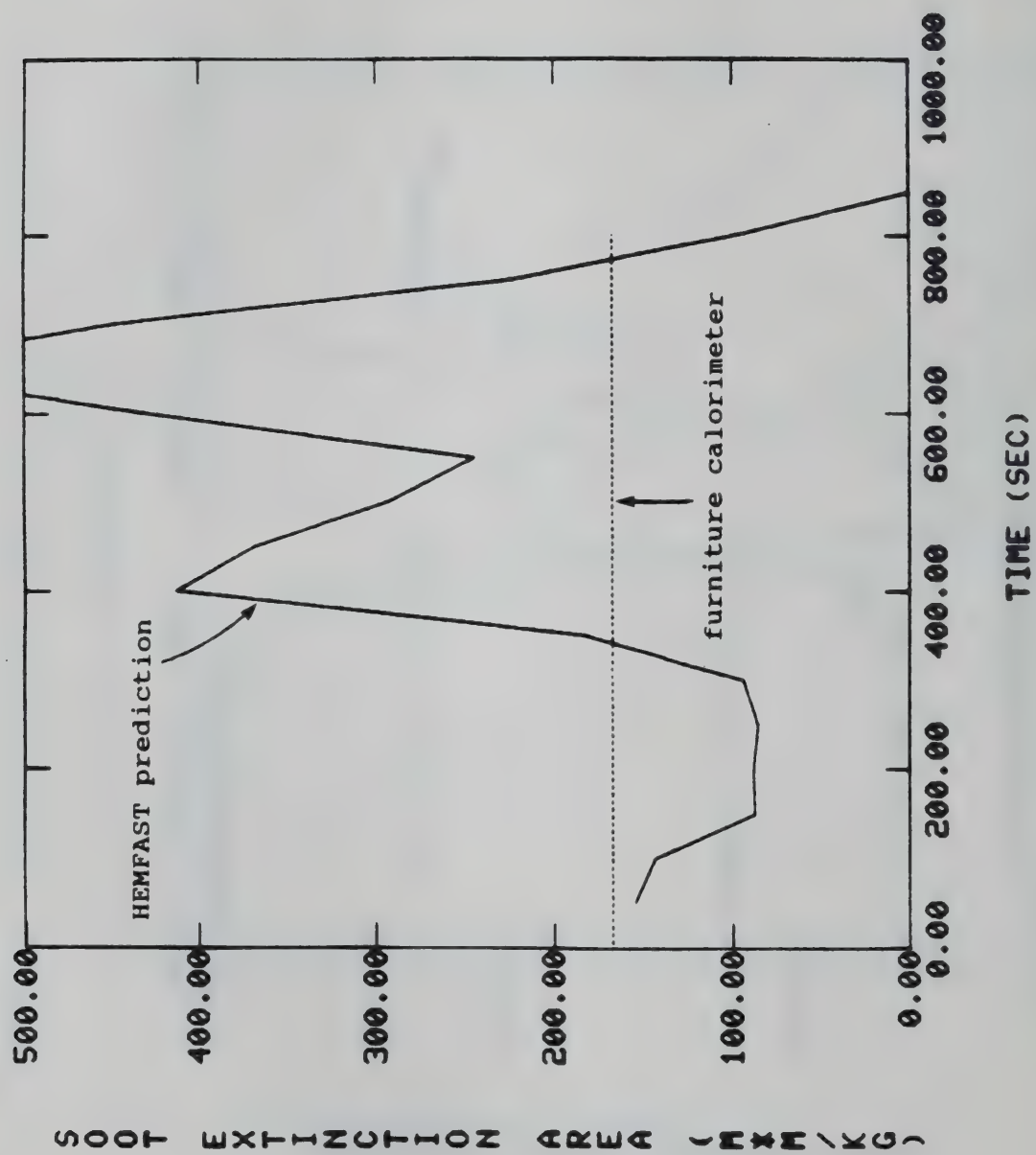Figure 27.   Mass loss rate comparison for HC/FRPU material

Figure 28. Soot extinction area comparison for HC/FRPU material

SECTION 5
CONCLUSIONS AND RECOMMENDATIONS

The HEMFAST model as described in Section 2 has potential for
flexibility, generality, and uniqueness. The current version can model a one
to four cushion mockup in a fire source room. A single material type is only
allowed but multiple flames can be simulated on a mockup. A simulation of a
building fire which include few mockup types, with a few material types, and
in different rooms is possible with minor programming changes of the model
geometrics without changing the models of the physical processes. The ability
to replace a module representing a physical process by an alternate module
without affecting other modules adds to the flexibility of the model. Thus
one can contemplate an engineering version on a smaller computer to simulate a
simple mockup fire in a single room. Or a research version can be
contemplated for a building fire with fire extinguishment for simulation on a
supercomputer.

The restructured model was designed to have good solution
predictability. First the bench scale data was converted to a derived
database that could be used directly by the HEMFAST calculation system. The
analysis of the couplings between the physical processes led to a numerical
scheme, summarized in Figure 8, that gave much improved solution stability,
accuracy, and efficiency. More specificly, the weakly coupled variables of
the surface temperature, the flame spread, and the burn history were solved by
effective numerical integrations. Meanwhile the coupled variables of
pyrolysis rates, burnrates, soot production, and thermal radiation were solved
in an iterative scheme at a fixed time. Certain output values of the
furniture fire model were linearly interpolated and processed for immediate
use by the FAST model. The implementation of the numerical schemes in the
model contributed to the significant program restructuring. The efforts in
minimizing the interfaces between FAST and FFM also significantly affected by
this restructuring.

The choice of a 4-cushion mockup with three different materials
challenged the model's predictability. Only a single material parameter, used
in the flame spread rate formula, needed calibration with the HEMFAST code
itself. The parameter is associated with the conductive heat rate from the

anchored diffusion flame and is determined from a fit to the horizontal flame spread data. The model validation involved four data sets for each material in which the model and the fire test data were compared. The comparison for the burn areas of the four cushions demonstrated the importance of including local transient radiative preheating of the material in the model. It was found that both processes of flame spreading and of the thermal ignitions need to be simulated to obtain good agreement with the cushion's burn area data. The rise in the burnrate and the peak burnrate value were predicted quite well by the model in the second set of data. The prediction of the furniture mass loss rate as a function of time in the third data set seemed about as good as the burnrate comparison. In the fourth data set, the model provides reasonable predictions of the soot extinction areas. Despite some good comparisons obtained so far, there is still room for improvements in the bench scale fire testing and in the modeling of the physical processes. These improvements can be implemented in the HEMFAST model without altering the model and the program architecture.

The computer code and the input/output data on magnetic tapes was delivered to NIST in early August 1988. Work has already begun on the third version of HEMFAST with a view toward usage by the fire safety community. There will be a full model documentation. The mockup construction will be generalized to create more variations as well as numbers of mockups and to have the capability for selecting a material for a panel of a mockup. The processing of the cone calorimeter data and of the flame spreading data will be improved to eventually remove the developer from the loop. That is, the calibration of material and scaling parameters should be done automatically by the bench scale processing routines without user interaction. Finally, some recent models of thermal heating, ignition and flame spread developed for real porous composite materials should be implemented in the model.

Future possibilities with the model could be inclusion of oxygen vitiation effects, an active fire suppression process, a more general fire plume model that includes some chemical kinetics, etc. Other possibilities include interfacing FFM program with the newer versions of FAST or with the Harvard CFC. These model improvements will require closer collaboration with other model developers.

SECTION 6

REFERENCES

1. Jones, W. W., "A Model for the Transport of Fire, Smoke, and Toxic Gases (FAST), NBSIR-84-   , July 1984.

2. Dietenberger, M. A., "Mathematical Modeling of Furniture Fires," NBS-GCR-86-506, February, 1986.

3. Dietenberger, M. A., "Description and Results of Furniture Fire Modules within FAST (HEMFAST)," UDR-TR-87-29, University of Dayton Research Institute, January 1987.

4. Dietenberger, M. A., "Improved Furniture Fire Model within 'FAST: HEMFAST," UDR-TR-87-135, University of Dayton Research Institute, October 1987.

5. Babrauskas, V. amd Krasny. J., "Fire Behavior of Upholstered Furniture," NBS Monograph 173, November 1985.

6. Mitler, H. B. and Emmons, H. W., "Documentation for CFC V, the Fifth Harvard Computer Fire Code," NBS-GCR-81-344, October 1981.

7. deRis, J. N., "Spread of a Laminar Diffusion Flame," Twelfth Symposium (International) on Combustion, The Combustion Institute, 1969, pp. 241-252.

8. Fernandez-Pello, A. K., Ray, S. R., and Glassman, I., "Flame Spread in an Opposed Flow: The Effect of Ambient Oxygen Concentration," 18th Symposium (International) on Combustion, The Combustion Institute, 1981, pp. 579-589.

9. Altenkirch, R. A., Eichhorn, R., and Shang, P. C., "Buoyancy Effects on Flames Spreading Down Thermally Thin Fuels," Combustion and Flame, Vol. 37, 1980, pp. 71-83.

10. Altenkirch, R. A., Eichhorn, R., and Rizni, H. R., "Correlating Downward Flame Spread Rates for Thick Fuel Beds," Combustion Science and Technology, Vol. 32, 1983, pp. 49-66.

11. Wichman, I. S. and Williams, F.A., "Simplified Model of Flame Spread in an Opposed Flow Along a Flat Surface of a Semi-Infinite Solid," Combustion Science and Technology, Vol. 32, 1983, pp. 91-123.

12. Quintiere, J., Harkleroad, M., and Hasemi, Y., "Wall Flames and Implications for Upward Flame Spread," DOT/FAA/CT-85/2, June 1985.

13. Al-Rabeh, A. H., "Embedded DIRK Methods for the Numerical Integration of Stiff Systems of ODEs," International J. Computer Math., Vol. 21, 1987, pp. 65-84.

14. Babrauskas, V., "Bench-Scale Methods for Prediction of Full-Scale Fire Behavior of Furnishing and Wall Linings," (SFPE-TR-84-10), 1984.

15. Krasny, J.F. and Babrauskas, V., "Burning Behavior of Upholstered Furniture Mockups," in J. of Fire Sciences, Vol. 2, May/June 1984, pp. 205-235.

16. Bukowski, R.W. and Braun, E., "Hazard I. Volume3: Data Base Listing," (NBSIR-87-3604), July 1987.

17. Babrauskas, V., Lawson, J.R., Walton, W.D., and Twilley, W.H., "Upholstered Furniture Heat Release Rates Measured with a Furniture Calorimeter," (NBSIR-82-2604), Dec. 1982.

18. Braun, E., Levin, B.C., Paabo, M., Gurman, J., Holt, T., and Steel, J.S., "Fire Toxicity Scaling," (NBSIR-87-3510), February 1987.

19. Seng-Chuan Tan, "Transient Horizontal Flame Spread Tests on Cellular Plastics - Experimental Results: Vols. 1, 2, & 3," (NBS-GCR-83-445 (&446)), October 1983.

20. Harkleroad, M., Quintiere, J., and Walton, W., "Radiative Ignition and Opposed Flow Flame Spread Measurements on Materials," DOT/FAA/CT-83-28, August 1983.

FORM NBS-114A (REV.11-84)

U.S. DEPT. OF COMM. **BIBLIOGRAPHIC DATA** **SHEET** (See instructions)	1. PUBLICATION OR REPORT NO. NIST/GCR-89/564	2. Performing Organ. Report No.	3. Publication Date June 1989

4. TITLE AND SUBTITLE

A Validated Furniture Fire Model with FAST (HEMFAST)

5. AUTHOR(S)

Mark A. Dietenberger

6. PERFORMING ORGANIZATION (If joint or other than NBS, see instructions) University of Dayton Research Institute Dayton, OH 45469	7. Contract/Grant No. Grant No. 60NANBSD0556
	8. Type of Report & Period Covered

9. SPONSORING ORGANIZATION NAME AND COMPLETE ADDRESS (Street, City, State, ZIP)

National Institute of Standards
   and Technology
U.S. Department of Commerce
Gaithersburg, MD 20899

10. SUPPLEMENTARY NOTES

☐ Document describes a computer program; SF-185, FIPS Software Summary, is attached.

11. ABSTRACT (A 200-word or less factual summary of most significant information. If document includes a significant bibliography or literature survey, mention it here)

This technical document reports on the validation of the furniture fire model with the furniture calorimeter data and on the restructure of the program 'HEMFAST'. Significant restructuring of the model and its code resolve various problems associated with the first version of HEMFAST. Comprehensive descriptions of the current model and its code structure benefit the HEMFAST users. The descriptions include: (1) data processing of the bench scale fire tests database, (2) effective time integrations of surface temperatures, flame spreads, and burn time, (3) effective coupled solutions of pyrolysis rates, burnrates, soot production, and thermal radiation, and (4) the effective interfacing between the furniture fire model and FAST. The model is validated with fire tests for a 4-cushion mockup fire with three different fabric/foam cushion types. The comparisons include: (1) burn area fractions of each cushion as a function of time, (2) burnrate of the mockup as a function of time with fire test data from the furniture calorimeter, (3) mass loss rate of the furniture as a function of time, and (4) the overall levels of soot production.

12. KEY WORDS (Six to twelve entries; alphabetical order; capitalize only proper names; and separate key words by semicolons)

burning rate; computer programs; cushions; fire models; furniture; furniture calorimeters; soot; upholstered furniture; validation

13. AVAILABILITY	14. NO. OF PRINTED PAGES
☒ Unlimited ☐ For Official Distribution. Do Not Release to NTIS ☐ Order From Superintendent of Documents, U.S. Government Printing Office, Washington, DC 20402.	84
	15. Price
☒ Order From National Technical Information Service (NTIS), Springfield, VA 22161	$14.95

USCOMM-DC 85-6006